

CNO_{Na} and ¹²C/¹³C in giant stars of 10 open clusters ^{*}

R. Smiljanic¹, R. Gauderon², P. North², B. Barbuy¹, C. Charbonnel^{3,4}, and N. Mowlavi⁵

¹ Universidade de São Paulo, IAG, Rua do Matão 1226, Cidade Universitária, 05508-090, São Paulo, SP, Brazil
e-mail: [rodolfo;barbuy]@astro.iag.usp.br

² Laboratoire d'astrophysique, Ecole Polytechnique Fédérale de Lausanne (EPFL) - Observatoire de Sauverny - CH 1290 Versoix, Switzerland
e-mail: Pierre.North@epfl.ch

³ Geneva Observatory, University of Geneva, Chemin des Maillettes 51, CH-1290 Versoix, Switzerland
e-mail: Corinne.Charbonnel@unige.ch

⁴ LATT, CNRS UMR 5572, Université de Toulouse, 14 avenue Edouard Belin, F-31400 Toulouse Cedex 04, France

⁵ Observatoire de Genève - Integral Science Data Center, Chemin d'Ecogia 16 - CH 1290 Versoix, Switzerland
e-mail: Nami.Mowlavi@unige.ch

Received ; accepted

ABSTRACT

Context. Evolved low-mass stars ($0.8 \leq M/M_{\odot} \leq 2.5$) of a wide range of metallicity bear signatures of a non-standard mixing event in their surface abundances of Li, C, and N, and in their ¹²C/¹³C ratio. A Na overabundance has also been reported in some giants of open clusters but remains controversial. The cause of the extra-mixing has been attributed to thermohaline convection that should take place after the RGB bump for low-mass stars and on the early-AGB for more massive objects.

Aims. To track the occurrence of this process over a wide mass range, we derive in a homogeneous way the abundances of C, N, O, and Na, as well as the ¹²C/¹³C ratio in a sample of 31 giants of 10 open clusters with turn-off masses from 1.7 to 3.1 M_⊙. The sample includes red giants, clump giants, and early-AGB stars. We study the observational behavior of the abundances as well as the possible correlations between different elements and between the chemical abundances and stellar mass.

Methods. A model atmosphere analysis is conducted using high signal-to-noise ratio, high-resolution FEROS and EMMI spectra. We derive atmospheric parameters using Fe I and Fe II lines. We calculate abundances for Na, C, N, and O, as well as the ¹²C/¹³C ratio using spectral synthesis. For the elements Mg, Ca, Si, Sc, Ti, V, Cr, Co, and Ni, abundances are derived using equivalent widths.

Results. A group of first ascent red giants with $M/M_{\odot} \leq 2.5$ exhibits lower [N/C] ratios than those measured in clump giants of the same mass range, suggesting an additional increase in the [N/C] ratio after the first dredge-up. The sodium abundances corrected from NLTE are found to be about solar. [Na/Fe] shows a slight increase of 0.10 dex as a function of stellar mass in the 1.8 to 3.2 M_⊙ range covered by our sample, in agreement with standard first dredge-up predictions. Our results do not support previous claims of sodium overabundances as high as +0.60 dex. An anti-correlation between ¹²C/¹³C and turn-off mass is identified and interpreted as being caused by a post-bump thermohaline mixing. Moreover, we find low ¹²C/¹³C ratios in a few intermediate-mass early-AGB stars, confirming that an extra-mixing process also operates in stars that do not experienced the RGB bump. In this case, the extra-mixing possibly acts on the early-AGB, in agreement with theoretical expectations for thermohaline mixing.

Key words. Stars: abundances – Stars: evolution – Stars: interiors – Stars: atmospheres – Open Cluster and Associations: individual: IC 2714, IC 4756, NGC 2360, NGC 2447, NGC 3532, NGC 3680, NGC 5822, NGC 6134, NGC 6281, NGC 6633

1. Introduction

In the standard model of stellar evolution, convection is the only mechanism that can drive mixing in stellar interiors. In this context, the only expected mixing episode between the main sequence (MS) and the tip of the red giant branch (RGB) is the so-called first dredge-up (Iben 1965), a deep convective envelope that transports nuclear-processed material to the surface, as the star approaches and begins to climb the RGB.

During the MS, hydrogen burns by means of the pp-chain and the CNO-cycle. Proton-capture cycles that require higher temperatures, i.e., the NeNa and MgAl cycles, remain ineffective (Weiss & Charbonnel 2004), except in stars more massive than $\sim 25 M_{\odot}$ (Decressin et al. 2007; Prantzos et al. 2007). Thus, in low-mass stars, the material mixed by the first dredge-up in-

creases the photospheric abundances of ³He, ¹³C, and ¹⁴N and decreases that of ¹²C as a function of the initial stellar mass and metallicity (Charbonnel 1994). The surface abundance of these elements can thus be used to test our understanding of the stellar evolutionary mixing processes.

The observed surface abundances of subgiants and low-luminosity RGB stars have been shown to agree with values predicted by first dredge-up models (Charbonnel et al. 1998; Gratton et al. 2000). However, accumulating observational evidence indicates a further increase in N and decrease in Li, C, and ¹²C/¹³C for low-mass RGB stars just after the luminosity bump. This extra-mixing phenomenon has been detected in giants of both open (Gilroy 1989; Gilroy & Brown 1991; Luck 1994; Tautvaišienė et al. 2000, 2005) and globular clusters (Shetrone 2003; Pilachowski et al. 2003; Recio-Blanco & de Laverny 2007, and references therein), as well as in field stars (Snedden et al. 1986; Charbonnel et al. 1998; Gratton et al. 2000), including extremely metal-poor giants (Cohen et al.

Send offprint requests to: R. Smiljanic

* Observations collected at ESO, La Silla, Chile (programmes 56.A-0285 and 65.L-0026A).

2006; Spite et al. 2006), and in extragalactic systems such as the LMC (Smith et al. 2002) and Sculptor (Geisler et al. 2005). These observations suggest that we are witnessing the effects of a universal process that is independent of environment, able to operate at all metallicities (although possibly with different efficiencies), and connected to the luminosity bump (Charbonnel & Do Nascimento 1998).

Effects connected to rotation have long been suspected as being the origin of the extra-mixing, as first suggested by Sweigart & Mengel (1979). In particular, the most probable mechanism has been proposed to be the interaction between meridional circulation and turbulence induced by rotation, as derived by Zahn (1992) (see also Charbonnel 1995). However, the maximum-rotation induced mixing scenario developed by Chanamé et al. (2005), as well as the evolutionary models for low-mass, low-metallicity stars of Palacios et al. (2006), which take into account the transport of both angular momentum and chemicals induced by meridional circulation and shear turbulence self-consistently, show that these processes alone cannot explain the observations.

The 3D modeling of a low-mass RGB star by Dearborn et al. (2006) provided fresh insight into the physical mechanism involved. Based on these simulations, Eggleton et al. (2006) suggested that the process responsible was a molecular-weight inversion created by the $^3\text{He}(^3\text{He}, 2p)^4\text{He}$ reaction in the external part of the hydrogen-burning shell. Charbonnel & Zahn (2007a) identified the related transport mechanism as the double diffusive instability often referred to as thermohaline convection (Stern 1960; Ulrich 1972; Kippenhahn et al. 1980), and showed it to be able to reproduce the observed Li, C, and N abundances, as well as the carbon isotopic ratio in RGB stars after the bump, while simultaneously destroying most of the ^3He produced on the MS.

In addition to the extra-mixing event in low-mass stars at the RGB bump, Charbonnel & Balachandran (2000) suggested a possible extra-mixing episode in intermediate-mass stars ($2.5 \leq M/M_{\odot} \leq 5.0$) that undergo the equivalent of the bump only during the early-AGB phase, after He-core exhaustion. As discussed in Charbonnel & Balachandran (2000), these two instances of extra-mixing would be connected to the nature of the lithium-rich giants. Cantiello & Langer (2008) reported that thermohaline mixing can indeed be present during core helium-burning and beyond in stars that still have a ^3He reservoir.

On the observational side, it has long been discussed whether RGB extra-mixing could modify the abundances of heavier elements, namely Na, whose abundance in red giants has received considerable attention (Hamdani et al. 2000; Jacobson et al. 2007; Sestito et al. 2008, and references therein). Although some works have detected a sodium overabundance, some controversy still exists. For example, while Tautvaišienė et al. (2000) found giants of M67 to be sodium-enriched, Randich et al. (2006) did not find these overabundances and, moreover, showed unevolved stars in this same cluster to have the same sodium abundance as the evolved stars.

Additionally, few works in the literature determined carbon isotopic ratios in giant stars of open clusters (Gilroy 1989; Gilroy & Brown 1991; Luck 1994; Tautvaišienė et al. 2000, 2005). Only the last three of these studies also derived abundances of C, N, O, and Na. Obviously the simultaneous determination of all these elements in a homogeneous analysis is important in constraining the mixing mechanisms as well as their possible dependence on stellar mass. Gilroy (1989) and Gilroy & Brown (1991) found that giant stars in open clusters with turn-off masses lower than $2.2M_{\odot}$ showed

a decreasing carbon isotopic ratio with decreasing turn-off mass. On the other hand, Luck (1994) also found some stars with low carbon isotopic ratio among clusters with turn-off masses higher than $2.2M_{\odot}$. The latter stars might be connected to the extra-mixing during the early-AGB, as suggested by Charbonnel & Balachandran (2000). Tautvaišienė et al. (2000) found a small difference between the isotopic ratios of clump star and red giants in M67, although a similar difference was not found in stars of NGC 7789 by Tautvaišienė et al. (2005).

It is clear that much work is required both on the theoretical and observational sides to improve our knowledge of the mixing processes in low- and intermediate-mass giant stars. In the present paper, we increase significantly the number of giants in Galactic open clusters analyzed so far. We derive abundances of several elements, in particular C, N, O, and Na, as well as the $^{12}\text{C}/^{13}\text{C}$ ratio for a sample of clump and red giants of 10 open clusters. In Sect. 2, the observations are described. In Sect. 3, we discuss the determination of the atmospheric parameters, and in Sect. 4, we present the abundances. In Sect. 5, we determine the evolutionary state of each sample star, and in Sect. 6, we discuss the results and their implications. Our conclusions are drawn in Sect. 7.

2. Observations

Observations of 24 giants were conducted with the FEROS spectrograph (Kaufer et al. 1999) at the ESO 1.52m telescope at La Silla (Chile). FEROS is a fiber-fed echelle spectrograph that provides a full wavelength coverage of $\lambda\lambda$ 3500–9200 Å over 39 orders at a resolving power of $R = 48\,000$. All spectra were reduced using the FEROS pipeline software. Typical signal-to-noise ratios (S/N) ranged between 125 and 370 at 6700 Å.

We also reanalyzed spectra of the seven red giants of NGC 2360 and NGC 2447 first analyzed by Hamdani et al. (2000). These spectra were obtained in 1995 using the EMMI spectrograph attached to the ESO NTT 3.5m telescope at La Silla. The spectra have a wavelength coverage of $\lambda\lambda$ 4050–6650 Å with $R = 28\,000$. The S/N varies between 73 to 236 at 6600 Å. The log book of the observations is given in Table 1. The table includes the V magnitude of the Geneva photometry when available, and from UBV photometry otherwise, the $[B - V]$ index of the Geneva photometry, the $B - V$ of the Johnson UBV photometry, and the signal-to-noise ratio per pixel of the extracted spectra for the specified wavelength. The adopted numbering follows the WEBDA database¹. We also give the HD, DM or Tycho-2 identifications when available, or numbers in the system of (Eggen 1968) for NGC 2360. The Julian Dates refer to the middle of the exposure. The exposure times are also listed.

2.1. Sample clusters

The data of the open clusters included in the sample are listed in Table 2. The $[\text{Fe}/\text{H}]^2$ value is the average of all values obtained for individual stars in this work. The other adopted parameters, $(m-M)$, $E(B-V)$, age, and distance, of NGC 2360 and NGC 2447, are the same as those listed by Hamdani et al. (2000). For NGC 6134, we adopt the parameters determined by

¹ The WEBDA database is a large database for stars in Galactic open clusters developed by Jean-Claude Mermilliod and now maintained by Ernst Paunzen of the Institute of Astronomy of the University of Vienna. The database can be accessed in the internet at the address: <http://www.univie.ac.at/webda/>

² $[A/B] = \log [N(A)/N(B)]_{\star} - \log [N(A)/N(B)]_{\odot}$

Table 1. Log book of the observations.

Star	DM or Eggen No	V	[B-V]	B-V	S/N	around [Å]	JD -2450000	t _{exp} [s]
IC 2714.05		11.046	0.582	1.263	184	6701	1730.511	5000
IC 4756.12	+05° 3805	9.473	0.500	1.030	174	6701	1731.751	1800
IC 4756.14	+05° 3808	8.813	0.737	0.860	197	6701	1732.750	1800
IC 4756.28	+05° 3818	8.970		1.360	166	6701	1730.703	1500
IC 4756.38	+05° 3829	9.756	0.416	1.100	237	6701	1730.731	2700
IC 4756.69	+05° 3850	9.201	0.366	1.060	271	6701	1730.755	1800
NGC 2360.7	8	11.087	0.294	1.000	89	6600	30.741	1800
NGC 2360.50	67	11.082	0.311	1.030	108	6600	30.767	2700
NGC 2360.62	81	11.272	0.251	0.940	73	6600	31.730	3600
NGC 2360.86	110	10.787	0.309	1.020	181	6600	31.822	3600
NGC 2447.28	-23° 6102	9.849	0.226	0.930	170	6600	30.847	1800
NGC 2447.34		10.123	0.197	0.900	236	6600	32.755	3000
NGC 2447.41		10.031	0.204	0.935	226	6600	32.840	2700
NGC 3532.19	-58° 3090	7.711	0.241	0.962	214	6701	1730.462	600
NGC 3532.100	-58° 3092	7.483	0.404	1.098	171	6701	1730.474	600
NGC 3532.122	-58° 3077	8.161	0.234	0.934	371	6701	1731.464	900
NGC 3532.596	-58° 2968	7.930		0.991	367	6701	1732.463	800
NGC 3532.670	-57° 4320	7.042		1.340	149	6701	1732.473	500
NGC 3680.13	-42° 6963	10.824	0.491	1.150	200	6701	1731.503	5000
NGC 5822.01		9.061	0.653	1.286	126	6701	1731.544	1500
NGC 5822.201		10.242	0.341	1.052	175	6701	1730.567	3600
NGC 5822.240	133519	9.468	0.728	1.336	128	6701	1731.569	2100
NGC 5822.316		10.455	0.375	1.031	175	6701	1732.617	2700
NGC 5822.443		9.720		1.220	177	6701	1731.600	2700
NGC 6134.30	8320-1928-1	11.840		1.270	200	6701	1730.646	7200
NGC 6134.99	8320-0960-1	11.633		1.357	168	6701	1732.673	6300
NGC 6134.202	8320-0965-1	11.619		1.464	146	6701	1731.690	7200
NGC 6281.03	322660	7.959	0.436	1.115	236	6701	1731.627	900
NGC 6281.04	322658	8.126	0.457	1.133	232	6701	1731.640	900
NGC 6633.078	170053	7.304	0.845	1.430	157	6701	1732.717	600
NGC 6633-100	170174	8.307	0.434	1.110	194	6701	1732.731	1000

Bruntt et al. (1999). For the other clusters, new parameters were determined in this work using UBV photometry obtained from the WEBDA database, and Geneva isochrones (Schaller et al. 1992) with metallicity $Z = 0.020$. Two values of the turn-off mass were determined using the corresponding Schaller et al. (1992) isochrone. The blue turn-off was defined to be the bluest limit of the isochrone, excluding the very short-lived phase just after core-H exhaustion, as indicated by point B in Fig. 1 of Maeder & Meynet (1991). The red turn-off is defined to be the reddest point just before the short blueward excursion, as indicated by point R in Fig. 1 of Maeder & Meynet (1991). We also list the mass at the clump as given by the isochrones, where the clump is defined as the point of lowest luminosity after He ignition. Finally, the Galactocentric distance of the cluster given by Chen et al. (2003) is given. The color-magnitude diagrams and isochrones of all clusters are shown in Figs. 1 and 2, where our sample stars are identified as black dots.

3. Atmospheric parameters

3.1. Equivalent widths and atomic data

The atomic-line list adopted in this work is the same as the one used by Hamdani et al. (2000) with the addition of a few Fe II lines. For elements other than Fe, the same oscillator strengths (gfs) as used by Hamdani et al. (2000) were adopted. For the Fe II lines, the gfs are those renormalized by Meléndez & Barbuy (2009), and also used in Smiljanic et al. (2006). The Fe I gfs are preferentially taken from the critical compilation of data by Fuhr & Wiese (2006) complemented by

values from the NIST web database (Ralchenko et al. 2005). The solar iron abundance adopted for the calculations is the one recommended by Grevesse & Sauval (1998), $A(\text{Fe}) = 7.50$.

For the stars in common with Hamdani et al. (2000), new equivalent widths (Ws) were measured only for the additional Fe II lines, while the original measurements for the remaining lines were adopted. The new Ws were measured by fitting Gaussian profiles to the lines using IRAF³. The same normalization of the continuum as used in previous measurements was adopted, to ensure consistency between them. We refer the reader to the original work for further details of the line list and the data reduction.

For the new data, the fitting of the continuum and the measurement of the Ws were conducted using the PeakFit software. New Fe II lines were then added to the line list after these measurements, and in this case, new Ws of the Fe II lines were also determined by fitting Gaussian profiles with IRAF. The same continuum normalization was adopted in both cases. A comparison between the Fe II Ws measured with Peak Fit and IRAF showed excellent agreement. Lines with equivalent widths smaller than 10 mÅ and larger than 150 mÅ were not used in our analysis. The new equivalent widths measured in this work are listed in the Appendix, Tables A.1 to A.4.

³ IRAF is distributed by the National Optical Astronomy Observatory, which is operated by the Association of Universities for Research in Astronomy, Inc., under cooperative agreement with the National Science Foundation of the USA.

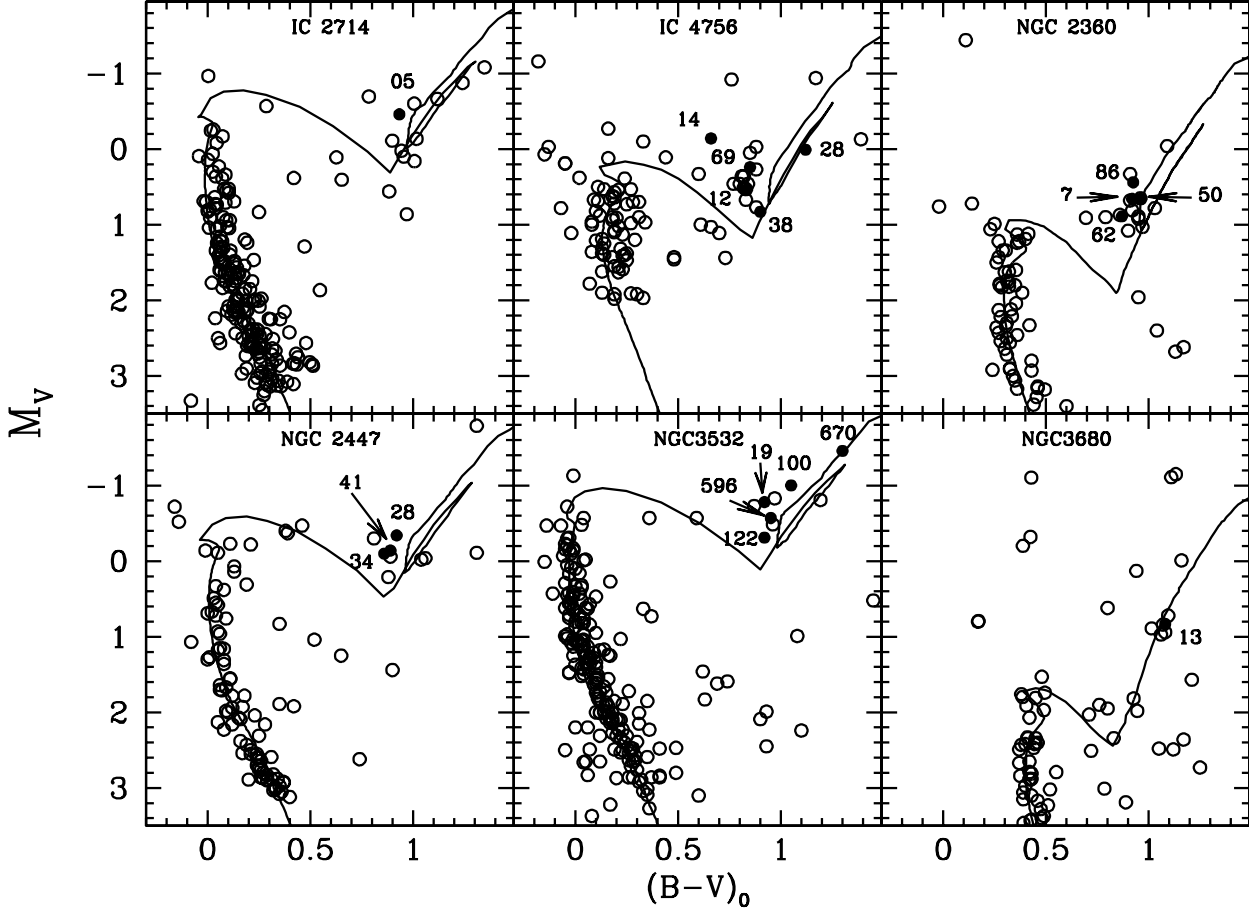


Fig. 1. The fitting of the color-magnitude diagrams of the clusters IC 2714, IC 4756, NGC 2360, NGC 2447, NGC 3532, and NGC 3680 with the isochrones by Schaller et al. (1992), used to determine the turn-off mass of the clusters (except for NGC 2360 and NGC 2447, see text). The observed stars are shown as full circles and are identified by their numbers. The parameters adopted for the fittings are the ones listed in Table 2.

Table 2. Physical data of the open clusters adopted from the literature or calculated in this work (see text).

Cluster	(m-M) (mag.)	E(B-V) (mag.)	E(b-y) (mag.)	Age (log yrs.)	Distance (pc)	[Fe/H]	$M_{\text{blue TO}}$ (M_{\odot})	$M_{\text{red TO}}$ (M_{\odot})	M_{clump} (M_{\odot})	R_{GC} (kpc)
IC 2714	11.50	0.33	–	8.60	1246	+0.12	2.55	2.85	2.91	8.34
IC 4756	9.00	0.20	–	8.85	474	+0.04	2.08	2.31	2.37	7.23
NGC 2360	10.40	0.07	–	9.06	1086	+0.04	1.78	1.98	2.02	6.32
NGC 2447	10.25	0.04	–	8.65	1057	–0.01	2.44	2.74	2.79	6.51
NGC 3532	8.50	0.04	–	8.55	473	+0.04	2.67	2.96	3.03	7.87
NGC 3680	10.07	0.07	–	9.25	935	+0.04	1.46	1.70	1.74	7.45
NGC 5822	9.65	0.14	–	8.95	697	+0.04	1.89	2.14	2.19	8.10
NGC 6134	–	–	0.263	8.85	1410	+0.12	2.08	2.31	2.37	7.52
NGC 6281	8.95	0.13	–	8.50	512	+0.05	2.78	3.09	3.18	8.47
NGC 6633	8.50	0.18	–	8.65	388	+0.08	2.44	2.74	2.79	8.42

3.2. Determination of the atmospheric parameters

Atmospheric parameters of the sample stars were determined using the standard spectroscopic approach. The effective temperature (T_{eff}) was calculated by assuming the excitation equilibrium of the Fe I lines (Fig. 3), i.e., requiring a null correlation between the iron abundance and the lower level excitation potential (χ). The surface gravity was found by assuming the ionization equilibrium of Fe, requiring both Fe I and Fe II lines to have the same

mean abundance (Fig. 3). The microturbulence velocity (ξ) was found by requiring the Fe I abundance to have a null correlation with the equivalent widths (Fig. 4). When these parameters are simultaneously constrained, the value of the metallicity, [Fe/H], is also determined. The parameters thus obtained are listed in Table 3.

When following this procedure, each time we converge to a set of parameters constrained by these criteria, the line list is checked for lines that indicate an abundance that departs by more

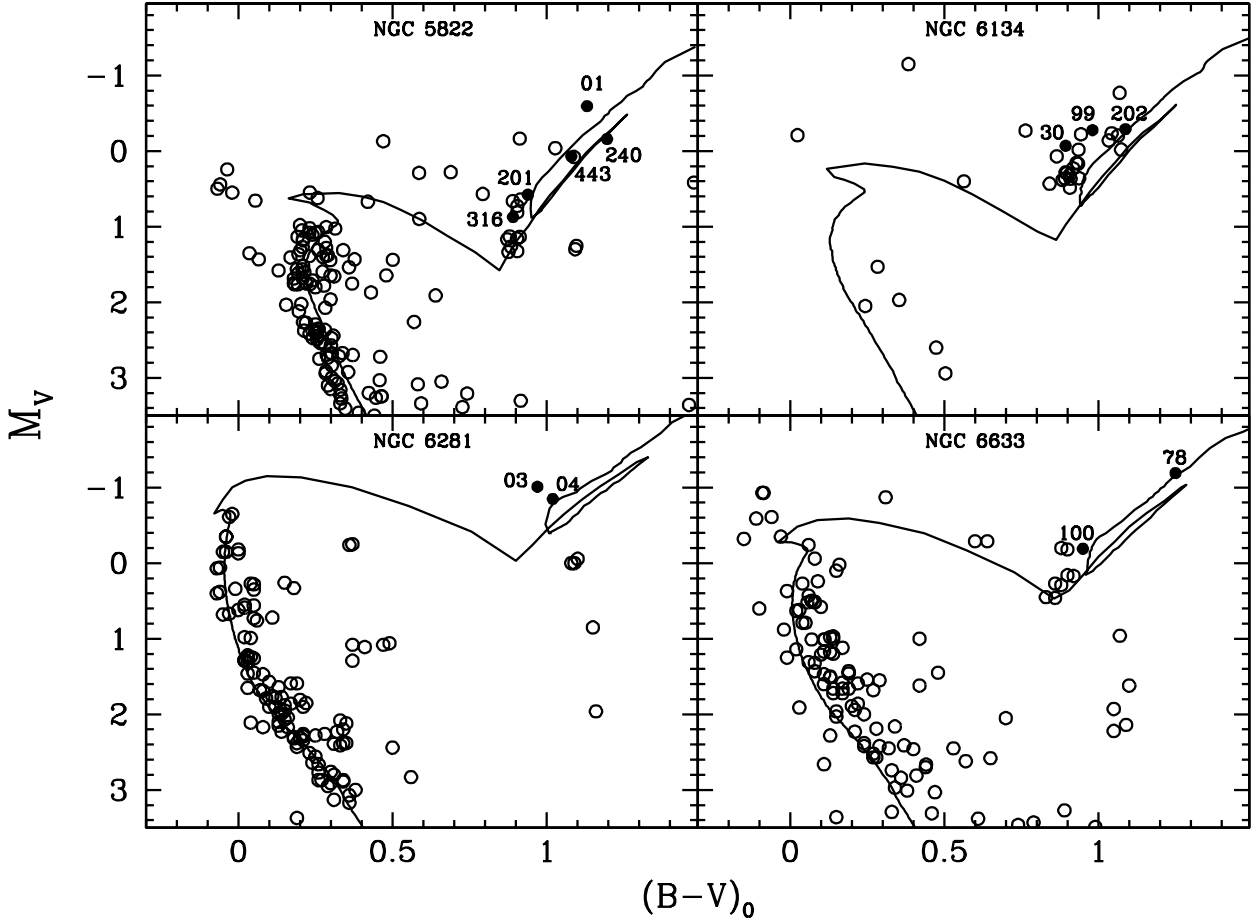


Fig. 2. The fitting of the color-magnitude diagrams of the clusters NGC 5822, NGC 6134, NGC 6281, and NGC 6633 with the isochrones by Schaller et al. (1992), used to determine the turn-off mass of the clusters (except for NGC 6134, see text). The observed stars are shown as full circles and identified by their numbers. The parameters adopted for the fittings are those listed in Table 2.

than 2σ from the average value. These lines are then excluded and a new set of parameters is calculated. The entire procedure is repeated until the abundance given by all lines agree to within 2σ . Thus, we believe to be excluding lines that are strongly affected by uncertain *gfs* or defective equivalent widths, and expect the mean abundance given by the remaining set of lines to be more reliable.

For these calculations, we adopted the grids of model atmospheres computed with the ATLAS9 code (Castelli & Kurucz 2003), without overshooting. The ATLAS9 models assume local thermodynamic equilibrium (LTE), plane-parallel geometry, and hydrostatic equilibrium.

3.3. Photometric temperatures

We calculated a photometric estimate of the effective temperature using the $(B-V)_0$ color as a way of testing our spectroscopically determined effective temperatures. The Johnson $(B-V)$ color was obtained from the WEBDA database and is listed in Table 1. The color excess listed in Table 2 was used to correct the observed color. Temperatures were calculated using the calibrations by Alonso et al. (1999) and Houdashelt et al. (2000). The average of these two estimates is listed in Table 3.

Temperatures calculated using the two photometric calibrations are in good agreement. The mean difference between them is 42 K. There is also good agreement between our spectroscopically determined T_{eff} and the average photometric value. The differences vary between 1 and 160 K, excluding the star IC 4756 14. The mean difference in the temperatures is 56 K. As detailed below, this is close to the uncertainty that we estimate for the spectroscopic temperature.

For star IC 4756 14, the difference between the photometric and spectroscopic temperatures is ~ 900 K, probably due to an incorrect $(B-V)$ color. The cluster IC 4756 is affected by differential reddening (Schmidt 1978; Smith 1983). We note that using a higher temperature we would infer a far higher metallicity, incompatible with the other cluster members. Therefore, the spectroscopic estimate is to be preferred.

This comparison shows that the spectroscopic method provides a reliable temperature scale. We therefore adopt these temperatures throughout the paper.

3.4. Evolutionary gravities

To test the spectroscopically determined gravities, we also determined $\log g$ values using the stellar masses obtained from the isochrone fittings. For this test, the stellar mass was con-

Table 3. The atmospheric parameters of the sample stars. The values for $[\text{Fe I}/\text{H}]$ and $[\text{Fe II}/\text{H}]$ are followed by the standard deviation and the number of lines on which the abundance is based. The spectroscopic values are the ones adopted throughout this work.

Star	T_{eff} (K) spectr.	T_{eff} (K) phot.	$\log g$ spectr.	$\log g$ evolut.	ξ (km s $^{-1}$)	$[\text{Fe I}/\text{H}] \pm \sigma$ (#)	$[\text{Fe II}/\text{H}] \pm \sigma$ (#)
IC 2714_5	5070	5020	2.70	2.49	1.50	+0.12 \pm 0.09 (38)	+0.12 \pm 0.04 (10)
IC 4756_12	5030	5189	2.75	2.79	1.37	-0.01 \pm 0.09 (39)	-0.01 \pm 0.06 (13)
IC 4756_14	4720	5627	2.47	2.36	1.57	+0.03 \pm 0.14 (41)	+0.03 \pm 0.08 (11)
IC 4756_28	4620	4548	2.42	2.36	1.41	+0.07 \pm 0.12 (39)	+0.07 \pm 0.09 (12)
IC 4756_38	5075	5056	3.00	2.92	1.21	+0.05 \pm 0.09 (41)	+0.05 \pm 0.07 (13)
IC 4756_69	5130	5158	3.00	2.71	1.31	+0.08 \pm 0.08 (42)	+0.08 \pm 0.06 (11)
NGC 2360_7	5115	5016	3.00	2.82	1.21	+0.11 \pm 0.11 (38)	+0.10 \pm 0.05 (10)
NGC 2360_50	5015	4897	2.90	2.77	1.37	-0.03 \pm 0.05 (27)	-0.02 \pm 0.11 (10)
NGC 2360_62	5105	5153	3.15	2.88	0.91	+0.12 \pm 0.08 (32)	+0.10 \pm 0.12 (13)
NGC 2360_86	4960	4906	2.65	2.62	1.18	-0.06 \pm 0.15 (40)	-0.07 \pm 0.03 (08)
NGC 2447_28	5060	5054	2.70	2.50	1.46	-0.01 \pm 0.14 (38)	0.00 \pm 0.08 (10)
NGC 2447_34	5120	5121	2.90	2.63	1.44	-0.01 \pm 0.12 (38)	-0.01 \pm 0.09 (11)
NGC 2447_41	5055	5028	2.80	2.57	1.37	-0.02 \pm 0.11 (37)	-0.02 \pm 0.09 (11)
NGC 3532_19	4995	5033	2.65	2.36	1.52	+0.11 \pm 0.11 (41)	+0.09 \pm 0.05 (12)
NGC 3532_100	4745	4731	2.15	2.13	1.66	+0.01 \pm 0.12 (37)	+0.02 \pm 0.05 (11)
NGC 3532_122	5045	5042	2.60	2.56	1.54	-0.02 \pm 0.11 (39)	-0.02 \pm 0.11 (11)
NGC 3532_596	5020	4943	2.50	2.44	1.58	+0.04 \pm 0.11 (41)	+0.04 \pm 0.09 (12)
NGC 3532_670	4355	4316	1.80	1.70	1.52	+0.08 \pm 0.11 (28)	+0.08 \pm 0.13 (11)
NGC 3680_13	4660	4684	2.60	2.58	1.30	+0.04 \pm 0.10 (38)	+0.06 \pm 0.12 (13)
NGC 5822_1	4470	4559	2.00	2.00	1.38	+0.03 \pm 0.10 (32)	+0.03 \pm 0.09 (11)
NGC 5822_201	5035	5035	2.85	2.78	1.32	+0.05 \pm 0.10 (44)	+0.06 \pm 0.06 (12)
NGC 5822_240	4425	4467	1.95	2.12	1.34	+0.02 \pm 0.11 (32)	+0.03 \pm 0.12 (11)
NGC 5822_316	5110	5125	3.05	2.92	1.28	+0.16 \pm 0.10 (43)	+0.16 \pm 0.03 (10)
NGC 5822_443	4610	4648	2.10	2.34	1.53	-0.06 \pm 0.11 (38)	-0.06 \pm 0.08 (12)
NGC 6134_30	4980	5138	2.95	2.99	1.23	+0.21 \pm 0.11 (41)	+0.21 \pm 0.08 (10)
NGC 6134_99	4785	4898	2.55	2.81	1.39	+0.10 \pm 0.10 (37)	+0.10 \pm 0.10 (12)
NGC 6134_202	4555	4677	2.25	2.67	1.34	+0.04 \pm 0.10 (34)	+0.06 \pm 0.12 (09)
NGC 6281_3	4915	4860	2.30	2.24	1.64	+0.01 \pm 0.09 (38)	+0.01 \pm 0.07 (13)
NGC 6281_4	5015	4855	2.50	2.35	1.70	+0.09 \pm 0.07 (33)	+0.09 \pm 0.04 (10)
NGC 6633_78	4370	4383	1.80	1.79	1.51	+0.04 \pm 0.10 (31)	+0.03 \pm 0.15 (12)
NGC 6633_100	5015	5016	2.85	2.56	1.44	+0.11 \pm 0.11 (42)	+0.11 \pm 0.08 (12)

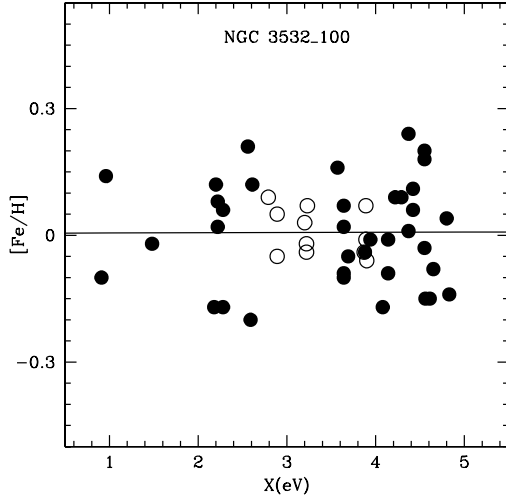


Fig. 3. Iron abundance of both Fe I (full circles) and Fe II lines (open circles) versus the line excitation potential for the star NGC 3532_100. The solid line is a linear fit to the Fe I lines indicating that the excitation equilibrium was fulfilled. The ionization equilibrium was also obtained by setting the Fe I and Fe II abundances to be equal, determining the surface gravity.

sidered to be equal to the stellar mass of the clump at the given

isochrone. Since there is little variation in mass between the red turn-off and the clump, this choice should introduce no important effect.

The evolutionary gravities were calculated using the classical equation, $\log g_{\star} = \log g_{\odot} + \log (M_{\star}/M_{\odot}) + 4 \log (T_{\text{eff}\star}/T_{\text{eff}\odot}) - \log (L_{\star}/L_{\odot})$, where $\log (L_{\star}/L_{\odot}) = -0.4 (M_{\text{bol}\star} - M_{\text{Bol}\odot})$. Luminosities were calculated with the parameters listed in Table 2 and bolometric corrections calculated with the relations by Alonso et al. (1999). For the Sun, we adopted $T_{\text{eff}} = 5777$ K, $\log g = 4.44$ dex, and $M_{\text{bol}} = 4.75$ mag. The gravities calculated in this way are given in Table 3.

The evolutionary $\log g$ is in good agreement with the spectroscopically determined $\log g$. The differences vary between 0.01 and 0.42 dex. The mean difference between the gravities is on the order of 0.14 dex. As discussed below, this is close to the uncertainty that we estimate for the spectroscopic gravity. Most of the spectroscopic values are systematically higher than the evolutionary ones. The disagreement between these two methods is well known in the literature and is also found for field giants when parallaxes are used to derive $\log g$ (Allende Prieto et al. 1999; da Silva et al. 2006). The precise reasons remain unknown, although departures from LTE are usually blamed. We consider it to be possible that our gravity values are systematically overestimated by an amount close to its associated uncertainty. This has little effect on the metallicities, since these are mainly derived from the gravity-insensitive Fe I lines.

This comparison again shows that the use of the spectroscopic method establishes a reliable gravity scale. We therefore adopt these gravities throughout the paper.

3.5. Uncertainties in the atmospheric parameters

The uncertainties in the atmospheric parameters were calculated for a representative star, IC 4756.14, whose atmospheric parameters are close to the median value for the entire sample. The 1σ uncertainties in T_{eff} and ξ were determined by the uncertainties in the linear fits used to constrain these parameters. The uncertainties were given by the variation in these parameters necessary to match the angular coefficient value of the linear fit to the value of its own uncertainty, in the diagram of Fe I abundance versus the line excitation potential for T_{eff} , and in the Fe I abundance versus W diagram for ξ . The 1σ uncertainty in the surface gravity was found by changing the gravity value until the difference between the mean abundances from Fe I and Fe II equals the larger of the standard deviation values.

The atmospheric parameters are not truly independent of each other and thus, for example, an error in the effective temperature may also introduce an error in the gravity. We thus also evaluated the influence of the uncertainty in each parameter on the remaining ones. This cross-terms were combined with the uncertainties calculated above to produce the total uncertainties caused by the analysis method, listed in the second column of Table 4.

Uncertainties in the measurement of the equivalent widths of the Fe I lines, caused by the S/N and the accuracy of the continuum definition, can also affect the calculation of the atmospheric parameters. After conducting some tests, we determined that the equivalent widths are affected by at most an uncertainty of $\sigma = \pm 3.0 \text{ m\AA}$. This uncertainty propagates into the atmospheric parameters at a level listed in the third column of Table 4.

In addition, we recalculated the parameters of three stars using a 2.5σ clipping factor, to test the influence of this choice on the derived atmospheric parameters. Some of the lines excluded before with 2σ were still excluded when using 2.5σ . After increasing the clipping factor, only a few extra lines were taken into account (from 3 to 9 Fe I lines), resulting mostly in similar parameters. The average differences in the atmospheric parameters calculated by adopting each of the two clipping factors are listed in the fourth column of Table 4. This was considered another source of uncertainty inherent to the method, and thus added to the other ones to calculate the final total uncertainty in the parameters.

The microturbulence velocity and the temperature were found to be mostly insensitive to the choice clipping factor, while $\log g$ was found to vary by a significant amount. This result shows that the addition of a few extra lines does not significantly affect the excitation equilibrium or the method used to constrain ξ . On the other hand, these extra lines do affect the mean abundances of Fe I and Fe II and thus force a change in $\log g$ to maintain the ionization equilibrium.

As a typical error in metallicity, we adopt the standard deviation in the Fe I values of star IC 4756.14, $\sigma_{[\text{Fe}/\text{H}]} = \pm 0.14$. This is one of the largest standard deviations, as seen in Table 3, and can thus be seen as a rather conservative choice. The effect of uncertainties related to the cross-terms (± 0.04), both the S/N and continuum (± 0.05), and the sigma-clipping procedure (± 0.03) have an almost negligible effect on the final total uncertainty in the metallicity (which would increase to ± 0.16).

Table 4. Uncertainties in the adopted atmospheric parameters.

Parameter	σ method	σ S/N & cont.	σ sigma-clip.	σ total
T_{eff} (K)	± 55	± 10	± 20	± 60
$\log g$ (dex)	± 0.20	± 0.07	± 0.15	± 0.26
ξ (km s $^{-1}$)	± 0.05	± 0.01	± 0.06	± 0.08

Other systematic effects might be present, because of the use of 1D stellar atmospheres, and the neglect of departures from the LTE, among others effects. These, however, are likely to affect all the sample stars in much the same way. Since we are mostly interested in a relative comparison between the stars, these effects do not significantly affect either the analysis or the conclusions. They might be important, however, when the results obtained here are compared to those obtained by other works in the literature.

3.6. Comparison with previous results

3.6.1. The sample of Hamdani et al. (2000)

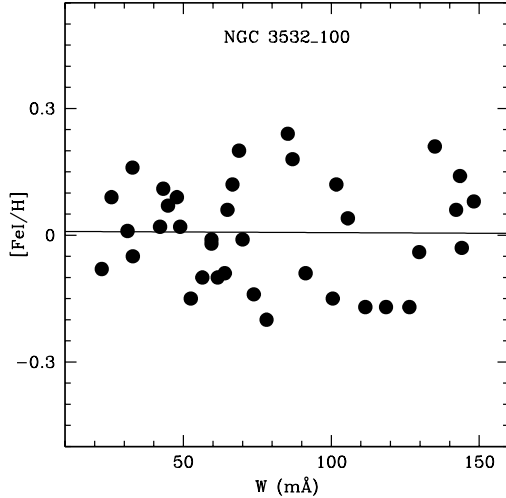
Although we use almost the same data as Hamdani et al. (2000), the methods that we employ to determine the atmospheric parameters are different. Hamdani et al. (2000) followed an iterative procedure, where the T_{eff} is given by minimizing the spread in the abundances of the iron-peak elements, and the surface gravity is calculated for this temperature and the masses given by the isochrones (see more details in the original paper). For reference, we list the parameters found by Hamdani et al. (2000) in Table 5.

Our temperatures are systematically lower than those found by Hamdani et al. (2000). The difference varies from 75 K to 170 K, with an average of ~ 125 K, larger than the estimated uncertainty. We believe that this systematic difference is related to a combination of the method and the final linelist. In particular, we note that, although we employ the same equivalent widths, our gf list is different. Our final Fe I mean abundance is also based on fewer lines. The first reason for that is the exclusion from the analysis of lines in the saturated part of the curve of growth, $W \geq 150 \text{ m\AA}$. A second reason is the σ -clipping procedure explained above. It seems that the lines we systematically exclude, in both the 2 or 2.5σ clipping, are the most significant causes for the different temperatures that we derive.

On the other hand, with the exception of one star, the gravities derived in this work are systematically higher than those adopted by Hamdani et al. (2000). The differences vary from 0.04 to 0.21 dex, with an average of 0.13 dex. The average difference is very close to the 1σ uncertainty estimated for $\log g$. While we rely on the ionization equilibrium, Hamdani et al. (2000) calculated the $\log g$ using the mass given by the isochrones and the known cluster distances. As discussed before, the spectroscopic method is known to result in systematically higher gravities. In addition, we note that this difference in $\log g$ does not seem to be related to the difference in temperature. An increase in the temperature of our stars would be followed by an increase in our $\log g$ values, which would only increase the discrepancies. The derived microturbulence velocity values behave in a similar way to the temperatures, probably for the same reason. We note that the range of our values is in excellent agreement with that found, for example, by da Silva et al. (2006) for field giants with a similar range of gravities and temperatures.

Table 5. Atmospheric parameters derived by Hamdani et al. (2000) for the stars in common with our sample.

Star	T_{eff}	$\log g$	ξ	$[\text{Fe I}/\text{H}] \pm \sigma$ (#)	$[\text{Fe II}/\text{H}] \pm \sigma$ (#)
NGC 2360_7	5230	2.89	1.57	$+0.15 \pm 0.17$ (57)	$+0.15 \pm 0.10$ (04)
NGC 2360_50	5170	2.86	1.69	$+0.01 \pm 0.17$ (55)	$+0.11 \pm 0.20$ (04)
NGC 2360_62	5180	2.94	1.44	$+0.08 \pm 0.17$ (52)	$+0.16 \pm 0.17$ (04)
NGC 2360_86	5130	2.73	1.52	$+0.04 \pm 0.16$ (55)	$+0.04 \pm 0.13$ (04)
NGC 2447_28	5140	2.56	1.75	-0.01 ± 0.21 (55)	$+0.06 \pm 0.16$ (04)
NGC 2447_34	5250	2.70	1.77	$+0.05 \pm 0.19$ (56)	$+0.03 \pm 0.13$ (04)
NGC 2447_41	5200	2.65	1.70	$+0.05 \pm 0.19$ (57)	$+0.04 \pm 0.16$ (04)

**Fig. 4.** Iron abundance versus W for the Fe I lines of NGC 3532_100. This plot was used to determine the microturbulence velocity by requiring a null correlation between $[\text{Fe I}/\text{H}]$ and the W s.

In spite of the different parameters, the metallicities ($[\text{Fe}/\text{H}]$) of the stars show good agreement with those of Hamdani et al. (2000). The average difference is $+0.05$ dex, a value well within the uncertainties. We believe this result to be evidence that reliable abundances can be derived regardless of small-scale differences introduced by the different methods of atmospheric-parameter calculation.

Gilroy (1989) appears to be the only other work that included another member of NGC 2360, star 12. It was found to have $[\text{Fe}/\text{H}] = +0.20$, a value that seems too high when compared with most of the metallicities obtained by us and by Hamdani et al. (2000). For NGC 2447, the only previous high-resolution analysis seems to be the one by Hamdani et al. (2000).

3.6.2. The new sample

In this section, we compare our results with literature data. We restrict the discussion to other analyses based on high-resolution spectra. In cases where the sample stars were targets of other analyses, the entire set of parameters is compared. A comparison of cluster metallicity is presented in cases where different cluster members were analyzed. To the best of our knowledge, this is the first time that atmospheric parameters and abundances have been derived for members of IC 2714 and NGC 6281 with high-resolution spectroscopy.

Members of IC 4756 were analyzed by Gilroy (1989), Luck (1994), and Jacobson et al. (2007). We have no star in common

with Luck (1994) and only IC 4756_69 in common with both Gilroy (1989) and Jacobson et al. (2007). While Gilroy (1989) found $T_{\text{eff}} = 5200$ K, $\log g = 3.20$, $\xi = 2.00$ km s $^{-1}$, and $[\text{Fe}/\text{H}] = 0.00$, in reasonable agreement with our parameters, except for the microturbulence, Jacobson et al. (2007) derived $T_{\text{eff}} = 5000$ K, $\log g = 2.20$, $\xi = 1.50$ km s $^{-1}$, and $[\text{Fe}/\text{H}] = -0.15$. While T_{eff} and ξ have close values, $\log g$ and $[\text{Fe}/\text{H}]$ are clearly discrepant. The reasons for this large discrepancy are probably related to the small number of Fe II lines used by Jacobson et al. (2007), only three. Our mean cluster metallicity, $[\text{Fe}/\text{H}] = +0.04$, is in good agreement with the ones found by Luck, $[\text{Fe}/\text{H}] = -0.03$, and Gilroy (1989), $[\text{Fe}/\text{H}] = +0.04$, while the mean metallicity derived by Jacobson et al. (2007), $[\text{Fe}/\text{H}] = -0.15$, disagrees with ours and those of other authors.

Three of the stars from NGC 3532, stars 19, 596, and 670, were also analyzed by Luck (1994). The parameters found by Luck (1994) are $T_{\text{eff}} = 5000$ K, $\log g = 2.36$, $\xi = 2.00$ km s $^{-1}$, $[\text{Fe}/\text{H}] = +0.13$ for star 19, $T_{\text{eff}} = 5000$ K, $\log g = 2.25$, $\xi = 2.00$ km s $^{-1}$, $[\text{Fe}/\text{H}] = +0.08$ for star 596, and $T_{\text{eff}} = 4500$ K, $\log g = 2.00$, $\xi = 2.40$ km s $^{-1}$, $[\text{Fe}/\text{H}] = +0.09$ for star 670. Temperatures and particularly the metallicities show good agreement, while our $\log g$ differ by 0.20 to 0.35 dex and the microturbulence velocities are systematically lower. The reason for this difference is unclear since the methods used in estimating $\log g$ and ξ were the same and the derived temperatures are similar. Our mean cluster metallicity is $[\text{Fe}/\text{H}] = +0.04$ in good agreement with the mean $[\text{Fe}/\text{H}] = +0.07$ found by Luck (1994).

Two high-resolution analysis of NGC 3680 members are reported in the literature, Pasquini et al. (2001) and Pace et al. (2008). The first work found an average of $[\text{Fe}/\text{H}] = -0.27$, although they considered the most accurate estimate to be $[\text{Fe}/\text{H}] = -0.17$ probably due to systematic effects. The latter work found $[\text{Fe}/\text{H}] = -0.04$, for two main-sequence stars. Our value for the only star that we analyze that is not included in these works, NGC 3680_13, is $[\text{Fe}/\text{H}] = +0.04$, which agrees with Pace et al. (2008) within the uncertainties.

Among our sample stars in NGC 5822, only star 01 had been analyzed before with high-resolution spectroscopy by Luck (1994). The parameters adopted by Luck (1994) are $T_{\text{eff}} = 4800$ K, $\log g = 2.50$, $\xi = 2.50$ km s $^{-1}$, and $[\text{Fe}/\text{H}] = +0.13$, which are clearly different from ours. An increase of 300 K in our temperature would still cause disagreement between the parameters including a very high metallicity of $[\text{Fe}/\text{H}] = +0.33$. We favor our lower value of temperature, which would be in excellent agreement with the two photometric estimates, 4500 and 4450 K also listed but not adopted by Luck (1994).

None of the stars that we studied in NGC 6134 had been previously analyzed with high-resolution spectroscopy. Carretta et al. (2004) analyzed 6 stars in this cluster and found a mean metallicity of $[\text{Fe}/\text{H}] = +0.15$ in very good agreement with our mean metallicity, $[\text{Fe}/\text{H}] = +0.12$.

Of the two stars that we analyze in NGC 6633, star 100 was analyzed by both Gilroy (1989) and Valenti & Fischer (2005). Gilroy (1989) derived $T_{\text{eff}} = 4800$ K, $\log g = 2.70$, $\xi = 1.80$ km s $^{-1}$, and $[\text{Fe}/\text{H}] = 0.00$, while Valenti & Fischer (2005) derived $T_{\text{eff}} = 5245$ K, $\log g = 3.11$, and $[\text{Fe}/\text{H}] = +0.35$. Our results are in closer agreement with those of Gilroy (1989), although our microturbulence is smaller and the metallicity is higher.

4. Abundances

4.1. Abundances using equivalent widths

Abundances were calculated for the elements Mg, Si, Ca, Sc, Ti, V, Cr, Co, and Ni using equivalent widths. Lines weaker than 10 mÅ, largely affected by the S/N and uncertainties in the continuum normalization, and stronger than 150 mÅ, on the saturated part of the curve of growth, were not used. The resulting abundances are listed in Table 6. We adopt the solar abundances reported in Grevesse & Sauval (1998).

In this analysis, the hyperfine structure (HFS) of the lines of elements such as Mg, Sc, V, Mn, and Co was not taken into account. Thus, caution is necessary when comparing these abundances with those obtained in other analyses. A reliable comparison is possible only within the sample analyzed here.

Table 6 includes the standard deviation of the mean values when possible. In these cases, it is possible to note that all abundances agree with the solar ones to within 2σ . The only exception is the Cr abundances given by the Cr II lines in some stars. The abundance given by the ionized Cr lines is always higher than the one given by the neutral species. The same is also seen in the case of V. As discussed before, it is possible that our spectroscopic $\log g$ values are slightly overestimated. This would also overestimate the abundances given by the ionized lines. In the cases of Cr and V, the abundance given by the neutral species is more reliable and should be preferred.

Star IC 4756_69 was found by Mermilliod & Mayor (1990) to be a spectroscopic binary. This system has a long period, 1994 days, but a very circularized orbit of eccentricity 0.0043 (Mermilliod et al. 2007). Assuming a mass of $2.37 M_{\odot}$ for the primary, a minimum mass of $0.59 M_{\odot}$ is estimated for the secondary, which is consistent with a possible white-dwarf nature.

The possible white-dwarf nature of the secondary, the extremely circularized orbit, and the abundance anomalies are all consistent with there having been a past mass-transfer event in the system. The orbital elements, in particular, are consistent with those observed for barium stars by Jorissen et al. (1998). Barium stars are also enriched in carbon and s-process elements (see Smiljanic et al. 2007, and references therein). Star 69, however, was not found to be enriched in carbon and s-process elements compared to the other stars in the same cluster. This implies that the mass-transfer event occurred before the companion star reached the thermal pulses in the AGB phase and enriched itself with the products of s-process nucleosynthesis.

4.2. Abundances using spectrum synthesis

The $^{12}\text{C}/^{13}\text{C}$ ratio and the abundances of C, N, O, and Na were derived using spectrum synthesis. The codes for calculating synthetic spectra are described by Barbuy et al. (2003) and Coelho et al. (2005). We adopted the solar abundances for C, N, and Na as recommended by Grevesse & Sauval (1998), $A(\text{C}) = 8.52$, $A(\text{N}) = 7.92$, and $A(\text{Na}) = 6.33$. For O, we adopted the abundance suitable to the 1D atmospheric models recommended by Allende Prieto et al. (2001), $A(\text{O}) = 8.77$.

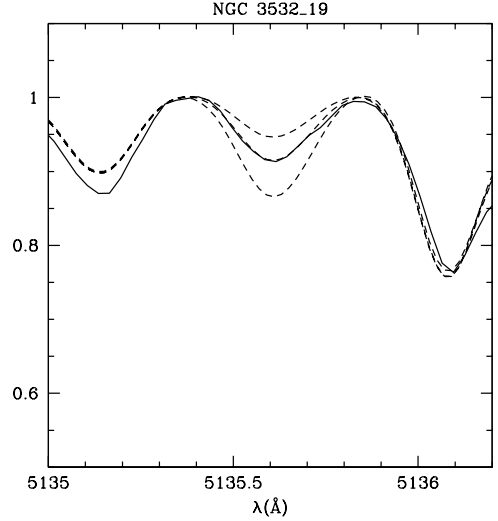


Fig. 5. Fit to the C_2 λ 5135.62 Å feature in NGC 3532_19. The observed spectrum is shown as a solid line. Synthetic spectra with $[\text{C}/\text{Fe}] = -0.11, -0.21$, and -0.31 are shown as dashed lines.

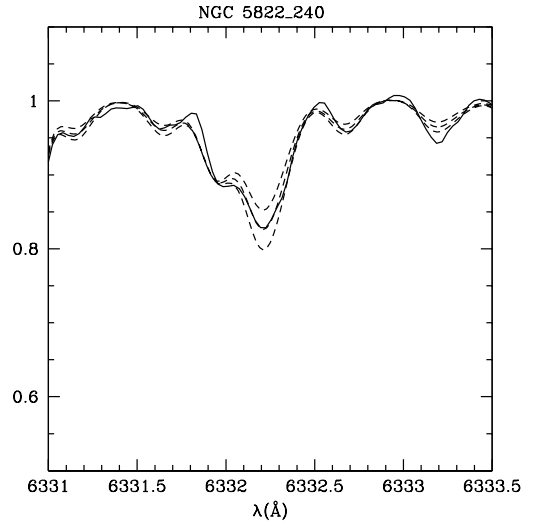


Fig. 6. Fit to the CN λ 6332.18 Å feature in NGC 5822_240. The observed spectrum is shown as a solid line. Synthetic spectra with $[\text{N}/\text{Fe}] = +0.23, +0.33$, and $+0.43$ are shown as dashed lines.

The carbon abundance was calculated using the $\text{C}_2(0,1)$ bandhead of the Swan system at λ 5135 Å. The data of the C_2 molecule are those adopted by Barbuy (1985), i.e., dissociation potential $D_0(\text{C}_2) = 6.21$ eV and electronic-vibrational oscillator strength $f_{00} = 0.0184$. We consider the C abundance derived from this feature to be the sum $^{12}\text{C} + ^{13}\text{C}$. An example of the fit is shown in Fig. 5.

The nitrogen abundance was derived using the $\text{CN}(5,1)$ λ 6332.18 Å bandhead of the $\text{A}^2\Pi - \text{X}^2\Sigma$ red system. The parameters for the atomic and molecular lines are the same as those used by Smiljanic et al. (2006) and Milone et al. (1992), i.e., dissociation potential $D_0(\text{CN}) = 7.65$ eV and electronic oscillator strength $f_{el} = 6.76 \times 10^{-3}$. An example of the fit is shown in Fig. 6.

Table 6. Mean elemental abundances for the program stars, followed by the standard deviation, when applicable, and the number of lines on which the abundance is based.

[X/Fe]	2714_5	4756_12	4756_14	4756_28	4756_38	4756_69
Mg	-0.02 (01)	-0.02 (01)	-0.05 (01)	-0.06 (01)	-0.05 (01)	-0.07 (01)
Si	+0.03 ± 0.12 (07)	+0.04 ± 0.09 (07)	+0.10 ± 0.07 (07)	+0.10 ± 0.09 (07)	+0.01 ± 0.06 (06)	+0.02 ± 0.04 (06)
Ca	+0.04 ± 0.04 (06)	+0.07 ± 0.10 (07)	+0.03 ± 0.05 (05)	-0.05 ± 0.04 (05)	+0.04 ± 0.09 (07)	+0.04 ± 0.09 (07)
Sc	-0.05 (02)	+0.01 (02)	+0.19 (02)	+0.02 (02)	+0.03 (02)	+0.07 (02)
Ti	-0.03 ± 0.09 (08)	-0.04 ± 0.11 (09)	-0.03 ± 0.16 (09)	-0.06 ± 0.05 (07)	-0.04 ± 0.10 (09)	-0.06 ± 0.04 (07)
V I	+0.04 ± 0.11 (08)	+0.03 ± 0.14 (08)	+0.09 ± 0.12 (08)	+0.01 ± 0.15 (08)	-0.06 ± 0.08 (07)	-0.05 ± 0.07 (06)
V II	+0.08 (02)	+0.19 (02)	+0.39 (02)	+0.22 (02)	+0.16 (02)	+0.19 (02)
Cr I	-0.01 ± 0.16 (13)	+0.03 ± 0.08 (15)	+0.11 ± 0.10 (13)	-0.04 ± 0.18 (15)	+0.05 ± 0.08 (15)	+0.03 ± 0.09 (14)
Cr II	+0.06 ± 0.11 (04)	+0.16 ± 0.10 (04)	+0.27 ± 0.08 (04)	+0.20 ± 0.12 (04)	+0.14 ± 0.06 (04)	+0.21 ± 0.11 (04)
Co	+0.05 ± 0.13 (08)	+0.05 ± 0.11 (08)	+0.12 ± 0.15 (08)	+0.05 ± 0.19 (08)	+0.02 ± 0.14 (08)	+0.06 ± 0.14 (08)
Ni	+0.01 ± 0.06 (09)	-0.02 ± 0.05 (10)	+0.03 ± 0.09 (09)	-0.01 ± 0.05 (07)	-0.02 ± 0.05 (11)	-0.01 ± 0.05 (10)

[X/Fe]	3532_19	3532_100	3532_122	3532_596	3532_670	3680_13
Mg	-0.07 (01)	-0.03 (01)	-0.03 (01)	0.00 (01)	-	-0.23 (01)
Si	+0.06 ± 0.06 (07)	+0.14 ± 0.09 (07)	+0.08 ± 0.16 (07)	+0.09 ± 0.11 (07)	+0.14 ± 0.11 (06)	+0.10 ± 0.09 (07)
Ca	+0.10 ± 0.12 (07)	+0.02 ± 0.06 (05)	+0.15 ± 0.12 (07)	+0.13 ± 0.11 (07)	+0.04 ± 0.04 (03)	+0.01 ± 0.04 (05)
Sc	-0.04 (02)	-0.07 (02)	-0.08 (02)	+0.04 (02)	+0.12 (02)	+0.08 (02)
Ti	-0.01 ± 0.08 (08)	-0.04 ± 0.08 (07)	-0.03 ± 0.13 (09)	-0.02 ± 0.10 (09)	+0.01 ± 0.09 (06)	-0.01 ± 0.04 (07)
V I	-0.01 ± 0.09 (07)	-0.04 ± 0.13 (08)	+0.05 ± 0.10 (07)	+0.02 ± 0.14 (08)	+0.16 ± 0.16 (07)	+0.09 ± 0.15 (08)
V II	+0.16 (02)	+0.14 (02)	+0.16 (01)	+0.14 (02)	+0.36 (02)	+0.24 (02)
Cr I	0.00 ± 0.10 (13)	-0.04 ± 0.11 (13)	+0.06 ± 0.17 (15)	+0.03 ± 0.06 (11)	-0.01 ± 0.13 (12)	0.00 ± 0.13 (13)
Cr II	+0.17 ± 0.08 (04)	+0.12 ± 0.06 (04)	+0.06 ± 0.11 (04)	+0.19 ± 0.05 (04)	+0.28 ± 0.21 (04)	+0.18 ± 0.06 (04)
Co	+0.03 ± 0.13 (08)	+0.01 ± 0.14 (08)	+0.12 ± 0.14 (08)	+0.10 ± 0.18 (08)	+0.13 ± 0.25 (07)	+0.14 ± 0.19 (08)
Ni	-0.01 ± 0.07 (09)	0.00 ± 0.07 (09)	-0.01 ± 0.08 (10)	-0.01 ± 0.09 (09)	+0.16 ± 0.15 (09)	+0.02 ± 0.08 (09)

Table 6. continued.

[X/Fe]	5822_1	5822_201	5822_240	5822_316	5822_443	6134_30
Mg	-	-0.01 (01)	-	-0.02 (01)	+0.03 (01)	0.00 (01)
Si	+0.13 ± 0.12 (07)	+0.06 ± 0.07 (07)	+0.11 ± 0.09 (06)	-0.04 ± 0.04 (06)	+0.17 ± 0.08 (07)	+0.03 ± 0.10 (07)
Ca	-0.02 ± 0.06 (03)	+0.03 ± 0.15 (07)	0.00 ± 0.08 (03)	0.00 ± 0.06 (06)	+0.06 ± 0.14 (06)	+0.06 ± 0.14 (06)
Sc	+0.03 (02)	0.00 (02)	+0.03 (02)	-0.17 (02)	+0.06 (02)	+0.10 (02)
Ti	-0.02 ± 0.08 (07)	+0.04 ± 0.04 (07)	-0.01 ± 0.08 (07)	-0.02 ± 0.10 (09)	-0.04 ± 0.06 (07)	-0.04 ± 0.06 (08)
V I	+0.11 ± 0.16 (08)	+0.05 ± 0.14 (08)	+0.12 ± 0.15 (07)	0.00 ± 0.08 (07)	+0.02 ± 0.13 (08)	-0.04 ± 0.05 (07)
V II	+0.28 (02)	+0.11 (02)	+0.27 (02)	+0.13 (02)	+0.26 (02)	+0.17 (02)
Cr I	-0.03 ± 0.17 (14)	+0.06 ± 0.10 (15)	+0.02 ± 0.07 (10)	+0.03 ± 0.10 (15)	+0.04 ± 0.10 (13)	+0.04 ± 0.09 (10)
Cr II	+0.11 ± 0.15 (04)	+0.16 ± 0.09 (04)	+0.16 ± 0.12 (04)	+0.19 ± 0.12 (04)	+0.19 ± 0.06 (04)	+0.20 ± 0.13 (04)
Co	+0.06 ± 0.20 (08)	+0.10 ± 0.15 (08)	+0.12 ± 0.20 (08)	+0.03 ± 0.15 (07)	+0.08 ± 0.15 (08)	+0.11 ± 0.16 (07)
Ni	+0.05 ± 0.09 (09)	+0.01 ± 0.06 (09)	+0.08 ± 0.13 (09)	-0.03 ± 0.05 (09)	+0.05 ± 0.05 (08)	+0.03 ± 0.10 (10)

[X/Fe]	6134_99	6134_202	6281_3	6281_4	6633_78	6633_100
Mg	-0.02 (01)	+0.01 (01)	+0.04 (01)	+0.02 (01)	-	-0.06 (01)
Si	+0.09 ± 0.08 (07)	+0.16 ± 0.11 (07)	+0.13 ± 0.07 (07)	+0.10 ± 0.07 (07)	+0.10 ± 0.09 (06)	+0.04 ± 0.08 (07)
Ca	+0.05 ± 0.08 (06)	+0.09 ± 0.16 (05)	+0.10 ± 0.11 (06)	+0.11 ± 0.10 (06)	-0.03 ± 0.08 (03)	-0.01 ± 0.05 (06)
Sc	+0.11 (02)	+0.02 (02)	-0.02 (02)	-0.01 (02)	+0.12 (02)	+0.11 (02)
Ti	0.00 ± 0.07 (07)	-0.06 ± 0.07 (07)	+0.01 ± 0.10 (07)	-0.03 ± 0.12 (09)	+0.05 ± 0.07 (07)	-0.03 ± 0.10 (09)
V I	+0.10 ± 0.13 (08)	+0.05 ± 0.16 (08)	-0.02 ± 0.08 (07)	+0.04 ± 0.12 (08)	+0.16 ± 0.16 (07)	-0.04 ± 0.07 (07)
V II	+0.28 (02)	+0.20 (02)	+0.15 (02)	+0.12 (02)	+0.40 (02)	+0.30 (02)
Cr I	+0.09 ± 0.11 (13)	+0.06 ± 0.14 (13)	+0.01 ± 0.08 (13)	+0.02 ± 0.10 (13)	0.00 ± 0.15 (12)	+0.03 ± 0.11 (13)
Cr II	+0.22 ± 0.10 (04)	0.00 ± 0.13 (04)	+0.15 ± 0.06 (04)	+0.14 ± 0.06 (04)	+0.27 ± 0.12 (04)	+0.25 ± 0.09 (04)
Co	+0.08 ± 0.17 (08)	+0.14 ± 0.14 (07)	+0.07 ± 0.18 (09)	+0.02 ± 0.14 (08)	+0.17 ± 0.23 (08)	+0.07 ± 0.16 (08)
Ni	+0.05 ± 0.08 (09)	+0.07 ± 0.08 (09)	+0.01 ± 0.06 (08)	+0.06 ± 0.06 (08)	+0.09 ± 0.14 (09)	-0.03 ± 0.08 (10)

The oxygen abundance was calculated from the [OI] 6300.311 Å forbidden line. The forbidden line is blended with a weak Ni I line at λ 6300.34 Å, which is included in the synthesis with parameters recommended by Allende Prieto et al. (2001). It also has a nearby Sc II line at λ 6300.70 Å for which we adopted the hyperfine structure by Spite et al. (1989). An example of the fit is shown in Fig. 7.

The $^{12}\text{C}/^{13}\text{C}$ ratio was derived by fitting the ^{12}CN and ^{13}CN lines in the $\lambda\lambda$ 8000-8006 Å region. The molecular data are the same as those adopted by da Silva et al. (1995) and described in Barbuy et al. (1992). An example of the fit to this region is shown in Fig. 8. As a check, we determined the $^{12}\text{C}/^{13}\text{C}$ ratio in the spectrum of Arcturus, adopting the atmospheric parameters and CNO abundances by Meléndez et al. (2003). The value that we obtained is $^{12}\text{C}/^{13}\text{C} = 6$, in excellent agreement with

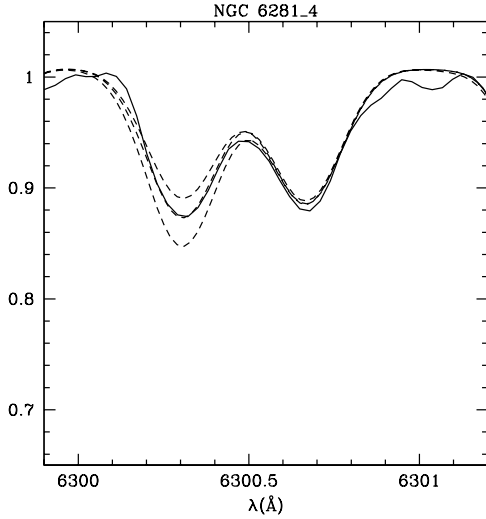


Fig. 7. Fit to the forbidden [OI] feature in λ 6300 Å in NGC 6281_4. The observed spectrum is shown as a solid line. Synthetic spectra with $[\text{O}/\text{Fe}] = -0.18, -0.08,$ and $+0.02$ are shown as dashed lines.

other literature results (see for example Charbonnel et al. 1998 and references therein).

The Na abundance was derived by fitting the Na I lines at λ 6154.23 Å and 6160.753 Å. We adopted the line parameters determined by Barbuy et al. (2006) by fitting the solar spectrum, i.e., $\log gf = -1.56$, $C_6 = 0.90 \times 10^{-31}$ and $\log gf = -1.26$, $C_6 = 0.30 \times 10^{-31}$, respectively. An example of the fit to the line λ 6154 Å is shown in Fig. 9.

Several works have estimated the influence of departures from the LTE on sodium abundances. In general, it is found that the lines at λ 6154/6160 Å are less affected and that the effects are stronger for metal-poor stars (Baumüller et al. 1998; Gratton et al. 1999; Mashonkina et al. 2000; Takeda et al. 2003; Shi et al. 2004). For these two lines, Baumüller et al. (1998) estimated a correction between 0.00 and -0.04 dex for the Sun, in good agreement with the -0.04 dex, for λ 6154 Å, and -0.06 dex, for λ 6160 Å, estimated by Takeda et al. (2003), who tabulated an extensive grid of NLTE corrections for a large range of atmospheric parameters. From these same grids, an average correction of -0.07 dex to λ 6154 Å and -0.11 dex to λ 6160 Å would correspond to the range in parameters of our sample, or -0.03 and -0.05 in the comparison with the Sun for the lines λ 6154 Å and 6160 Å, respectively. In Table 7, we list the mean $[\text{Na}/\text{Fe}]$ already corrected for NLTE effects.

4.3. Uncertainties in the abundances

An important source of uncertainties in the abundances are the uncertainties in the determination of the atmospheric parameters. These were estimated by changing each atmospheric parameter by its uncertainty, keeping the others to their adopted values, and recalculating the abundances. In this way, we measured the effect of the parameter uncertainty on the abundance. The results are listed in Table 8. The total uncertainty was calculated by quadratically adding the individual uncertainties.

The carbon isotopic ratio is rather robust, as can be seen from Table 8, since both isotopic species are expected to react in similar ways to the change in the parameters. It is well known that only the uncertainty in the microturbulence velocity is usu-

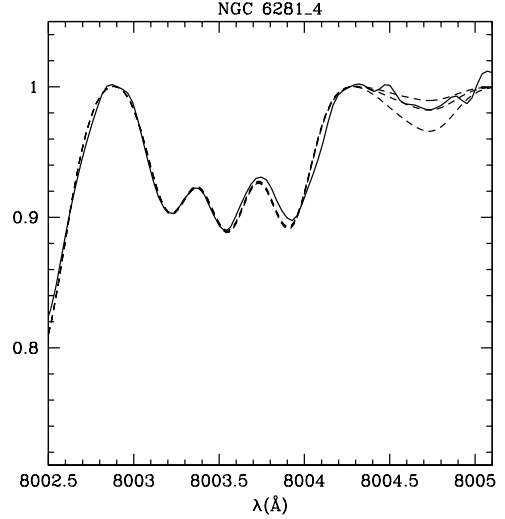


Fig. 8. Fit to the ^{12}CN and ^{13}CN features in the region of 8005 Å in NGC 6281_4. The observed spectrum is shown as a solid line. Synthetic spectra with $^{12}\text{CN}/^{13}\text{CN} = 06, 12,$ and 20 are shown as dashed lines.

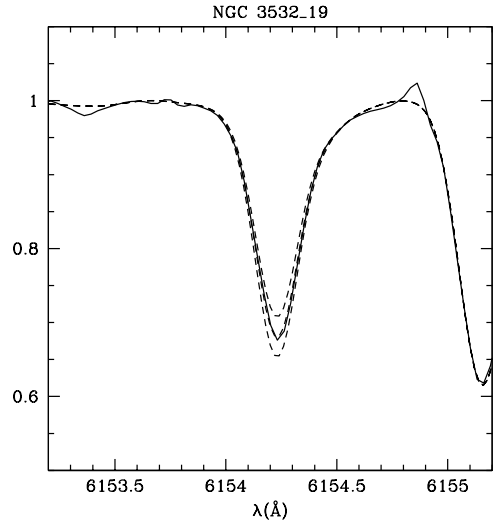


Fig. 9. Fit to the Na I line at 6154 Å in NGC 3532_19. The observed spectrum is shown as a solid line. Synthetic spectra with $[\text{Na}/\text{Fe}] = -0.10, 0.00,$ and $+0.10$ are shown as dashed lines.

ally important. In our case, however, the uncertainties that we estimate for these parameters are too small to introduce significant changes in the carbon isotopic ratio. For this ratio, the most important sources of uncertainties are the photon noise and the placement of the continuum.

The uncertainty due to photon noise was estimated as follows. The star IC 4756_14 was again used as a template, since its parameters lie close to the median defined by the sample. Using its atmospheric parameters and abundances, two synthetic spectra were calculated, one with $^{12}\text{C}/^{13}\text{C} = 10$ and the other with $^{12}\text{C}/^{13}\text{C} = 20$. Then, a Gaussian noise level equivalent to signal-to-noise ratios of 100, 200, and 350 (the range of S/N of the observed spectra) were introduced into each spectrum, producing six synthetic spectra. The $^{12}\text{C}/^{13}\text{C}$ ratio was then measured for each spectrum by searching for lower and upper values that would be considered reasonable fits. The difference between the original ratio and the upper and lower limits determined in this

Table 7. Abundances of Na, C, N, and O, and the $^{12}\text{C}/^{13}\text{C}$ ratio. We list the NLTE sodium abundances already corrected, as discussed in the text. The [N/C] ratio and the sums C+N, O+N, C+O, and C+N+O are also given.

Star	[Na/Fe]	[C/Fe]	[N/Fe]	[O/Fe]	$^{12}\text{C}/^{13}\text{C}$	[N/C]	C+N	O+N	C+O	C+N+O
IC 2714_5	0.00	-0.17	0.51	—	—	0.68	8.81	—	—	—
IC 4756_12	0.05	-0.14	0.50	-0.03	11	0.64	8.69	8.89	9.01	8.90
IC 4756_14	-0.02	-0.14	0.45	-0.01	17	0.59	8.71	8.94	9.05	8.94
IC 4756_28	-0.05	-0.15	0.32	-0.02	15	0.47	8.68	8.97	9.06	8.94
IC 4756_38	-0.01	-0.18	0.34	0.00	10	0.52	8.65	8.96	9.05	8.94
IC 4756_69	0.15	-0.60	0.55	-0.17	05	1.15	8.66	8.76	8.97	8.92
NGC 2360_7	-0.02	—	—	—	—	—	—	—	—	—
NGC 2360_50	0.02	-0.18	0.40	—	—	0.58	8.6	—	—	—
NGC 2360_62	-0.03	-0.24	0.22	—	—	0.46	8.64	—	—	—
NGC 2360_86	-0.03	-0.18	0.45	-0.10	—	0.63	8.60	8.78	8.90	8.79
NGC 2447_28	0.05	-0.18	0.58	-0.17	—	0.76	8.72	8.78	8.96	8.84
NGC 2447_34	0.03	-0.18	0.48	-0.13	—	0.66	8.66	8.81	8.95	8.83
NGC 2447_41	0.06	-0.15	—	-0.12	—	—	—	8.81	—	—
NGC 3532_19	-0.02	-0.25	0.34	-0.21	12	0.59	8.68	8.85	8.97	8.85
NGC 3532_100	0.05	-0.20	0.47	-0.13	10	0.67	8.67	8.82	8.96	8.84
NGC 3532_122	0.08	-0.15	0.48	—	—	0.63	8.67	—	—	—
NGC 3532_596	0.06	-0.22	0.40	-0.22	—	0.62	8.65	8.78	8.92	8.79
NGC 3532_670	0.08	-0.15	0.37	-0.08	20	0.52	8.71	8.94	9.04	8.92
NGC 3680_13	-0.07	—	—	—	—	—	—	—	—	—
NGC 5822_1	-0.05	-0.15	0.43	—	13	0.58	8.69	—	—	—
NGC 5822_201	0.03	-0.19	0.47	—	13	0.66	8.71	—	—	—
NGC 5822_240	-0.02	-0.10	0.33	—	17	0.43	8.66	—	—	—
NGC 5822_316	-0.07	-0.21	0.39	—	—	0.60	8.77	—	—	—
NGC 5822_443	-0.01	-0.13	0.50	—	10	0.63	8.65	—	—	—
NGC 6134_30	-0.03	-0.21	0.42	—	12	0.63	8.84	—	—	—
NGC 6134_99	0.07	—	—	—	—	—	—	—	—	—
NGC 6134_202	-0.02	-0.09	0.36	—	13	0.45	8.70	—	—	—
NGC 6281_3	0.09	-0.24	0.55	-0.15	12	0.79	8.70	8.79	8.97	8.86
NGC 6281_4	0.02	-0.22	0.40	-0.08	12	0.62	8.70	8.93	9.04	8.93
NGC 6633_78	-0.01	-0.17	0.38	-0.11	18	0.55	8.67	8.87	8.98	8.86
NGC 6633_100	-0.03	-0.19	0.45	-0.06	21	0.64	8.76	8.97	9.09	8.98

Table 8. The uncertainties in the abundances introduced by the uncertainties in the atmospheric parameters.

Elem.	σ_{Teff}	σ_{logg}	σ_{ξ}	$\sigma_{[\text{Fe}/\text{H}]}$	σ_{total}
Na	± 0.04	± 0.01	± 0.02	± 0.02	± 0.05
C	± 0.01	± 0.02	± 0.01	± 0.05	± 0.06
N	± 0.03	± 0.05	± 0.01	± 0.03	± 0.07
O	± 0.02	± 0.08	± 0.01	± 0.07	± 0.11
$^{12}\text{C}/^{13}\text{C}$	± 0.00	± 0.00	± 0.00	± 0.00	± 0.00

Table 9. Uncertainty in the $^{12}\text{C}/^{13}\text{C}$ ratio caused by the photon noise.

$^{12}\text{C}/^{13}\text{C}$	S/N	σ
10	100	$^{-1}_{+2}$
10	200	$^{-1}_{+1}$
10	350	$^{-0}_{+1}$
20	100	$^{-3}_{+2}$
20	200	$^{-2}_{+1}$
20	350	$^{-1}_{+2}$

way therefore provided a measurement of the uncertainty introduced by the photon noise and is listed in Table 9.

The uncertainty caused by the continuum placement was, again, estimated using the star IC 4756_14. The approach in this case was straightforward. The normalization of the continuum was repeated in the region of the ^{13}CN line, adopting different but yet reasonable points to define the pseudo-continuum. The carbon isotopic ratio was then redetermined in each case. The uncertainty related to the variations in the the continuum was estimated to be $\sigma = \pm 2$.

5. Evolutionary state of the sample stars

We used the isochrone fitting shown in Figs. 1 and 2 to derive the evolutionary status of each of the sample stars. The luminosity, evolutionary state, membership, and multiplicity of each of the sample stars are listed in Table 10.

IC 2714

For the relatively poorly studied southern Galactic cluster IC 2714, we adopted the numbering system of Becker (1960). Only the star IC 2714_5 was included in our sample. According to Clariá et al. (1994), IC 2714_5 is a confirmed member of the cluster based on kinematic and photometric criteria. As already noted by them, its position in the CMD (Fig. 1) indicates that the star is a clump giant in the core helium-burning phase.

IC 4756

Five stars of the Galactic cluster IC 4756 were included in our sample, IC 4756_12, 14, 28, 38, and 69, where we adopt the numbering system of Kopff (1943). Based on proper motions, Herzog et al. (1975) concluded that stars 38 and 69 have high probabilities of being members, while star 28 is a non-member.

Table 10. Luminosities, evolutionary stage, membership, and binarity of the sample stars.

Star	$\log(L/L_{\odot})$	Evol. Stage	Member	Binary
IC 2714_5	2.18	clump	m	–
IC 4756_12	1.78	clump	m	no
IC 4756_14	2.10	clump	m	no
IC 4756_28	2.06	RGB	nm/m	no
IC 4756_38	1.66	clump or RGB	m	no
IC 4756_69	1.89	clump	m	yes
NGC 2360_7	1.71	clump	m	no
NGC 2360_50	1.73	clump	m	no
NGC 2360_62	1.64	clump	m	yes
NGC 2360_86	1.85	clump or early-AGB	m	no
NGC 2447_28	2.16	clump	m	no
NGC 2447_34	2.04	clump	m	no
NGC 2447_41	2.09	clump	m	no
NGC 3532_19	2.31	clump	m	prob.
NGC 3532_100	2.44	early-AGB	m	no
NGC 3532_122	2.12	clump or RGB	nm/m	prob.
NGC 3532_596	2.23	clump	m	no
NGC 3532_670	2.72	early-AGB or RGB tip	m	prob.
NGC 3680_13	1.73	bump RGB or clump	m	no
NGC 5822_1	2.33	early-AGB	m	no
NGC 5822_201	1.76	clump	m	yes
NGC 5822_240	2.19	RGB	m	no
NGC 5822_316	1.64	clump	m	no
NGC 5822_443	2.04	RGB or early-AGB	m	prob.
NGC 6134_30	1.56	clump or early-AGB	m	yes
NGC 6134_99	1.68	clump or early-AGB	m	no
NGC 6134_202	1.73	RGB or early-AGB	m	no
NGC 6281_3	2.42	clump	m	–
NGC 6281_4	2.34	clump	m	–
NGC 6633_78	2.61	early-AGB	m	no
NGC 6633_100	2.08	clump	m	no

However, the values of its radial velocity measured in this work and by Mermilliod & Mayor (1990) implies that this star is a member of the cluster. All five sample stars were considered to be members by Mermilliod & Mayor (1990). The radial velocity monitoring by Mermilliod & Mayor (1990) also indicated that stars 12, 14, 28, and 38 are most probably single stars, while star 69 was shown to be a binary system with a period of 2000 days.

The color-magnitude diagram (Fig. 1) of this cluster should be interpreted with caution because it is affected by differential reddening (Schmidt 1978; Smith 1983). On the basis of their positions in the CMD, stars 12, 14, and 69 are possible clump giants, while star 28 seems to be a first-ascent red giant. Star 38 is either at the base of the RGB or in the clump.

NGC 2360

The four stars analyzed by Hamdani et al. (2000), NGC 2360_7, 50, 62, and 86, were included in our sample, where the numbering system of Becker et al. (1976) was adopted. All four stars were considered to be cluster members by Mermilliod & Mayor

(1990). They also found that stars 7, 50, and 86 are most probably single stars while, star 62 is a spectroscopic binary. Stars 7 and 86 were found by Baumgardt et al. (2000) to have a 72% probability of membership based on Hipparcos (ESA 1997) proper motions. The positions of the stars in the CMD (Fig. 1) seem to indicate that stars 07, 50, and 62 are clump giants, while star 86 might be a clump or an early-AGB star.

NGC 2447

The three stars of this cluster analyzed by Hamdani et al. (2000) were included in our sample, NGC 2447_28, 34, and 41, where the numbering system from Becker et al. (1976) was also adopted. Mermilliod & Mayor (1989) found that the three stars were cluster members with no evidence of binarity. The position of the stars in the CMD (Fig. 1) seems to indicate that they are clump giants (Clariá et al. 2005).

NGC 3532

Five stars in this cluster were also included in our sample, stars NGC 3532_19, 100, 122, 596, and 670, where we adopt the numbering system of Fernandez & Salgado (1980). According to González & Lapasset (2002), stars 19, 122, and 670 show probable variations in the radial velocities and might be binaries. Stars 100 and 596 do not exhibit radial-velocity variability and are possible single stars. Kinematically, González & Lapasset (2002) consider all five stars to be cluster members, although they flag star 670 with a doubtful membership because of its large distance from the cluster center. The photometric criteria by Clariá & Lapasset (1988) for assigning membership indicate that all stars except star 122 are cluster members.

As noted by Clariá & Lapasset (1988), the positions of the stars in the CMD (Fig. 1) seem to indicate that stars 19 and 596 are possible clump giants in the core helium-burning phase. Star 122 might be either a clump or an RGB star. Star 100 seems to be slightly more evolved, possibly on the early AGB. Star 670 is the most luminous star of our sample. It is above the luminosity expected for the end of the core helium-burning and is thus probably an AGB star. We note however that Clariá & Lapasset (1988) classified this same star as a tip RGB object, a possibility that we cannot exclude.

NGC 3680

Only one star of this cluster was included in our analysis, star NGC 3680_13, adopting the numbering system of Eggen (1969). Based on proper motions, Kozhurina-Platais et al. (1995) concluded that star 13 is a member of the cluster. Mermilliod et al. (1995) found no evidence of binarity and thus we consider star 13 to be a single star. Clariá & Lapasset (1983) classified the object as a core He-burning clump star. The isochrone that we used from Schaller et al. (1992) does not extend beyond the He flash. Based only in the CMD (Fig. 1), we identify NGC 3680_13 instead as a bump RGB star. However, we do not exclude the possibility of it being a clump giant.

NGC 5822

Five stars of this open cluster were included in our analysis, stars NGC 5822_1, 201, 240, 316, and 443, where we adopt the numbering system of Bozkurt (1974). According to Mermilliod & Mayor (1990), all five stars seem to be true mem-

bers of the cluster. In this same work, star 201 was found to be a spectroscopic binary and all other sample stars are most probably single stars. According to the CMD (Fig. 2), we classified stars 240 as a first ascent giant, stars 201 and 316 as clump stars, and star 01 as an early-AGB star. Star 443 might be either a RGB or an early-AGB star.

NGC 6134

Three stars in this cluster were included in our analysis, NGC 6134_30, 99, and 202, according to the numbering system of Lindoff (1972). According to Clariá & Mermilliod (1992), all three stars are members of the cluster, stars 99 and 202 are single stars and star 30 is a spectroscopic binary. According to their positions in the CMD (Fig. 2), stars 30 and 99 are probable clump or early-AGB stars, while star 202 might be a RGB or an early-AGB star.

NGC 6281

Two stars in this open cluster were included in our sample, NGC 6281_3 and 4, according to the numbering system of Feinstein & Forte (1974). The photometric criteria of Clariá et al. (1989) and the proper motions of Dias et al. (2001) indicate that both stars are cluster members. In the CMD (Fig. 2), both stars seem to be clump giants.

NGC 6633

Two stars of this open cluster are included in our sample, NGC 6633_78 and 100, where we adopt the numbering system of Kopff (1943). The proper motion study by Vasilevskis et al. (1958) indicated that star 100 is a member. The radial velocity measurements of Mermilliod & Mayor (1989) indicated that both stars are single stars and true members. According to their positions in the CMD (Fig. 2), star 100 is a clump giant and star 78 might be an early-AGB star.

6. Discussion

6.1. Carbon, nitrogen, and oxygen

When the material is processed by the CNO-cycle, the relative abundances of C, N, and O change, but the sum C+N+O should remain constant. In Table 7, we list the sums C+N, O+N, C+O, and C+N+O for the sample stars. The sum of C+N+O in our sample varies slightly from 8.79 to 8.98, with an average of 8.88 ± 0.06 . This value is close to the solar one, 9.00, and agrees with the almost solar average metallicity of our sample, $[\text{Fe}/\text{H}] = +0.05 \pm 0.06$. The agreement between stars in a given cluster is also excellent, confirming that the observed mixing effects on CNO abundances are the result of the CNO-cycle.

In Fig. 10, we plot the nitrogen abundances of the sample stars as a function of the carbon abundances. The isolated open square with high N and low C is star IC 4756_69, a binary star with a low-mass companion, probably a white dwarf. For this object, the observed CNO abundances (in reality, an upper limit for carbon and a lower limit for nitrogen) are compatible with those observed in more massive giants (Smiljanic et al. 2006) and are probably caused by a mass-transfer event in the system. We thus excluded IC 4756_69 from the following plots and discussion. The star with the lowest N content is NGC 2360_62 (starred symbol in Fig. 10), which is also a binary star. However, the reason for its low nitrogen abundance is unclear.

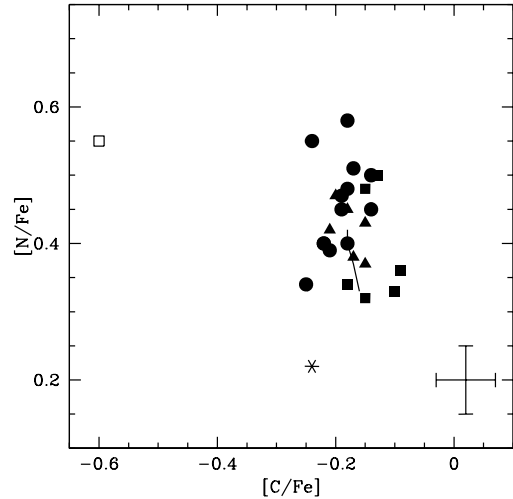


Fig. 10. Nitrogen abundances, $[\text{N}/\text{Fe}]$, as a function of the carbon abundances, $[\text{C}/\text{Fe}]$, for the sample stars. Star IC 4756_69 is shown as an open square, star NGC 2360_62 as a starred symbol. Possible RGB stars, including the ones with dubious classification, are shown as full squares, clump giants as full circles, and possible early-AGBs as full triangles. The solid line connects the values expected for stars between 1.7 and 4.0 M_{\odot} in the models of Schaller et al. (1992). A typical error bar is shown.

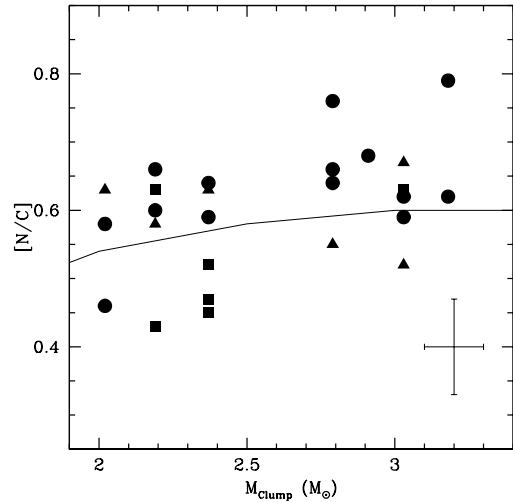


Fig. 11. $[\text{N}/\text{C}]$ ratio as a function of the mass of the clump stars. Possible RGB stars are shown as full squares, clump giants as full circles, and possible early-AGBs as full triangles. The solid line represents the predicted $[\text{N}/\text{C}]$ as a function of initial stellar mass given by the models of Schaller et al. (1992).

Excluding these 2 stars, one can note that there is no correlation between C and N; a correlation coefficient of $\rho = -0.14$ is found. The remaining stars have an average $[\text{C}/\text{Fe}] = -0.17 \pm 0.04$ and an average $[\text{N}/\text{Fe}] = +0.43 \pm 0.07$. The low rms values imply that the stars have very similar abundances. To discuss mixing, however, it is more appropriate to use the $[\text{N}/\text{C}]$ ratio rather than the N or C abundances. This ratio is given in Table 7. The sample has an average of $[\text{N}/\text{C}] = +0.61 \pm 0.08$, in excellent agreement with the ratio predicted after the first dredge-up by

the models of Schaller et al. (1992) for a star with $2.5 M_{\odot}$, $[\text{N}/\text{C}] = +0.58$ (Charbonnel 1994).

In Fig. 11, we plot the $[\text{N}/\text{C}]$ ratio as a function of the stellar mass at the clump of each cluster. The clump mass must be very close to the mass of the sample stars in the individual clusters. Only small differences are expected, as can be seen by comparing the mass at the red turn-off and the mass at the clump, as listed in Table 2. In the same figure, we show as a solid line the $[\text{N}/\text{C}]$ predicted by the models of Schaller et al. (1992) as a function of mass after the first dredge-up. A small increase in $[\text{N}/\text{C}]$ with stellar mass is predicted, in agreement with the observed behavior. A small difference in the average abundances on each side of the mass gap, between 2.4 and $2.8 M_{\odot}$, is suggested by the figure. The stars of lower mass have, on average $[\text{N}/\text{C}] = +0.57 \pm 0.08$, while the stars of higher mass have $[\text{N}/\text{C}] = +0.64 \pm 0.08$. Given the observational uncertainties, it is however difficult to judge whether this difference is real.

The stars in all figures of this section are plotted with different symbols according to their possible evolutionary stages. The group of stars with higher mass in Fig. 11 ($> 2.5 M_{\odot}$) mostly consist of more evolved clump (circles) and early-AGB stars (triangles). On the other hand, most less evolved RGB stars (squares) have masses lower than $2.5 M_{\odot}$. These less evolved stars tend to have lower $[\text{N}/\text{C}]$ ratios than clump and early-AGBs of the same mass.

The four RGB stars in the lower mass range with smaller $[\text{N}/\text{C}]$ are IC 4756_28, IC 4756_38, NGC 5822_240, and NGC 6134_202. The circle with low $[\text{N}/\text{C}]$ is star NGC 2360_62, the binary with an anomalous low N abundance. This group of four stars has an average of $[\text{N}/\text{C}] = +0.47 \pm 0.04$. The remaining, and possibly more evolved, stars with masses lower than $2.4 M_{\odot}$ have $[\text{N}/\text{C}] = +0.63 \pm 0.03$. In case the difference in the abundances is real, it might be related to the evolutionary status of the stars.

There are three other stars in the sample that could potentially be RGB stars based on the CMDs, NGC 3532_122, NGC 3680_13, and NGC 5822_443. We do not have the $[\text{N}/\text{C}]$ ratio for NGC 3680_13. Both of the other stars have $[\text{N}/\text{C}] = +0.63$. The higher $[\text{N}/\text{C}]$ value of these last two stars might argue they are not RGB stars but more evolved giants.

We note that the models by Schaller et al. (1992) may overestimate the effect of the first dredge-up for stars with $\sim 2.2 M_{\odot}$. For a $1.5 M_{\odot}$ star, Schaller et al. (1992) predict $[\text{N}/\text{C}] = +0.44$, closer to the average value of the RGB stars discussed above. Observations must thus be compared to predictions of models that include up-to-date initial abundances and solar mixtures. Work is in progress in that direction.

In Fig. 12, we show the oxygen abundances of the sample stars as a function of the $[\text{N}/\text{C}]$ ratio. A weak anti-correlation is evident with $\rho = -0.53$. This correlation was not detected by Smiljanic et al. (2006) for more massive stars, $M/M_{\odot} \geq 4$. However, the correlation was seen by Luck et al. (2006) for these more massive stars. Given the uncertainties, one needs to be cautious in these interpretations. Further analyses with larger samples are necessary before a conclusion can be made.

In Fig. 13, we show the $[\text{O}/\text{Fe}]$ ratio as a function of the stellar mass. The solid line represents the oxygen abundance in the models of Schaller et al. (1992) after the first dredge-up. Only a small change in $[\text{O}/\text{Fe}]$ is expected. Our results suggest a slightly more pronounced dependence with the mass. However, it is interesting that the stars on the theoretical curve belong to the same cluster, IC 4756. This includes two of the RGB stars, IC 4756_28 and 38, but also the clump giants IC 4756_12 and 14. If the effect that we observe is real, it seems to be an effect related to

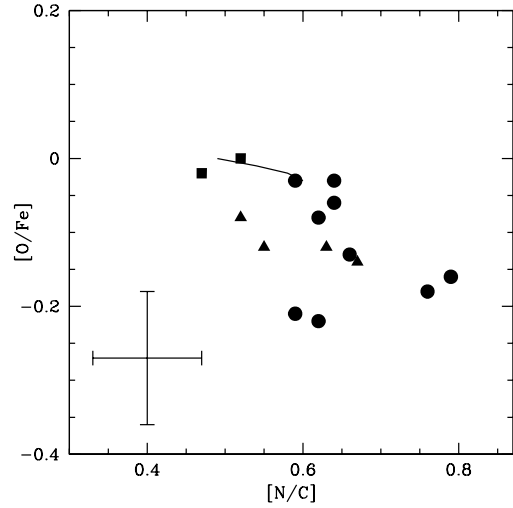


Fig. 12. The oxygen abundance of the sample stars as a function of the $[\text{N}/\text{C}]$ ratio. Star IC 4756_69 is not shown. Symbols are as in Fig. 11. The solid line connects the values expected for stars between 1.7 and $4.0 M_{\odot}$ in the models of Schaller et al. (1992). A typical error bar is shown.

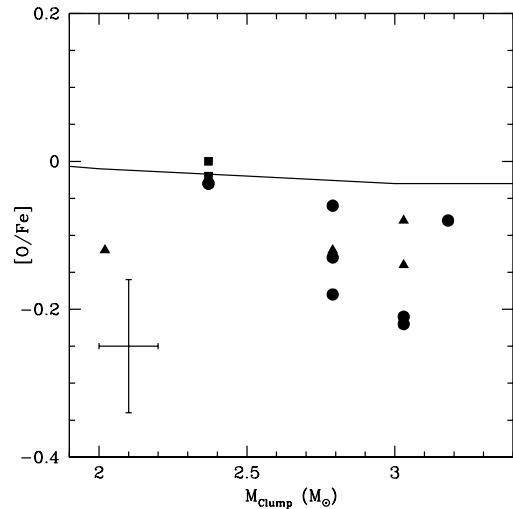


Fig. 13. The oxygen abundance of the sample stars as a function of the stellar mass at the clump. Symbols are as in Fig. 11. The solid line represents the predicted $[\text{O}/\text{Fe}]$ as a function of initial stellar mass given by the models of Schaller et al. (1992).

the stellar mass and not to an extra-mixing affecting giants with different evolutionary stages.

6.2. Sodium

Sodium abundances have been calculated for giants in a number of open clusters. Very different results have however been reported in the literature. Some works measured sodium overabundances of as high as $[\text{Na}/\text{Fe}] = +0.60$ (Jacobson et al. 2007), some reported only a mild overabundance of $[\text{Na}/\text{Fe}] = +0.20$ (Hamdani et al. 2000), and others reported solar or almost solar abundances (Sestito et al. 2007). Among the factors responsible for this discrepancy was the adoption of different gfs for the Na lines. For example, the values of gfs that

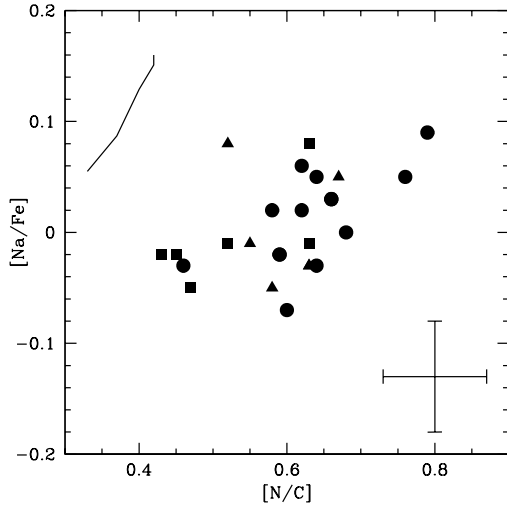


Fig. 14. Sodium abundance, $[\text{Na}/\text{Fe}]$, as a function of the $[\text{N}/\text{C}]$ ratio for the sample stars. Symbols are as in the previous figures. The solid line connects the values for $[\text{Na}/\text{Fe}]$ expected for stars between 1.8 and $4.0 M_{\odot}$ in the models of Mowlavi (1999) to the $[\text{N}/\text{C}]$ values of Schaller et al. (1992). A typical error bar is shown.

we adopt were derived with respect to the Sun for the lines λ 6154 Å and 6160 Å and by using a solar sodium abundance of $A(\text{Na}) = 6.33$ (Grevesse & Sauval 1998). These values are the same as those reported in the NIST database. They are 0.18 and 0.24 dex higher, respectively, than the values adopted by Jacobson et al. (2007), which had been derived with respect to Arcturus. Another factor is the adoption of different NLTE corrections, or even no correction. As discussed before, we adopted corrections in our analysis that are based on the work by Takeda et al. (2003).

In Fig. 14, we plot the sodium abundances derived in this work as a function of $[\text{N}/\text{C}]$. We obtain a correlation coefficient of $\rho = 0.49$, which indicates if anything only a weak correlation. The average sodium abundance of the sample is $[\text{Na}/\text{Fe}] = 0.01 \pm 0.05$, for the complete interval of $[\text{N}/\text{C}]$.

The sodium abundances are displayed in Fig. 15 as a function of stellar mass, together with the first dredge-up predictions from a standard evolution code (Mowlavi 1999; Hamdani et al. 2000). Both the observed and predicted abundances show an increase of about 0.10 dex over the mass range covered by our sample. A 2×2 contingency table was compiled with the limits $M_{\text{clump}} = 2.5$ and $[\text{Na}/\text{Fe}] = 0.00$. The two-tailed Fisher test yields a probability $P = 0.011$ that the samples are drawn from the same parent population, which demonstrates that the correlation is significant. The agreement would be perfect were it not for a slight offset of about 0.08 dex between the observed and predicted data. Since we do not expect the sodium surface abundance to decrease during the evolution of a star by means of the first and second dredge-ups, we may argue that our observed values are, on average, slightly underestimated by about 0.08 dex. While this remains within the margins of error, the most significant result of our data is the relative increase in the Na abundances as a function of stellar mass by an amount that agrees with model predictions.

In summary, our results do not support the claim by Jacobson et al. (2007, and references therein) of sodium overabundances as high as $+0.60$ in giants of open clusters, in

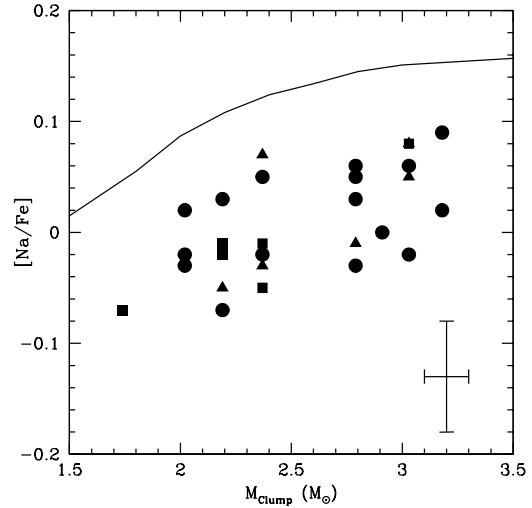


Fig. 15. Sodium abundances, $[\text{Na}/\text{Fe}]$, as a function of the mass of the clump stars. A typical error bar is shown. The solid line represents the predicted $[\text{Na}/\text{Fe}]$ as a function of initial stellar mass, given by the models of Mowlavi (1999).

agreement with the conclusions of Randich et al. (2006) and Sestito et al. (2007, 2008). Our results instead are consistent with a slight dependence, as predicted by standard stellar evolution models, of the sodium abundance at the surface of red giants on stellar mass.

6.3. $^{12}\text{C}/^{13}\text{C}$

Gilroy (1989) and Gilroy & Brown (1991) analyzed stars from 20 open clusters and showed that the $^{12}\text{C}/^{13}\text{C}$ ratio in giants of clusters with turn-off masses higher than $\sim 2.2 M_{\odot}$ agree with the expected behavior from standard first dredge-up models, $^{12}\text{C}/^{13}\text{C} \sim 20$ (Schaller et al. 1992) (see also Fig. 6 of Charbonnel 1994). They also found, on the other hand, that giants in clusters with turn-off masses lower than $\sim 2.2 M_{\odot}$ have a decreasing carbon isotopic ratio with decreasing turn-off mass.

Although Gilroy & Brown (1991) found no evidence in M67 for different carbon isotopic ratios between red giants and clump giants, Tautvaišienė et al. (2000) analyzing a larger sample of M67 clump giants found a small difference between the isotopic ratios of these two groups. A possible additional mixing after the He-core flash was suggested. A similar difference between clump and red giants, however, was not found by Tautvaišienė et al. (2005) in NGC 7789.

In Fig. 16, we plot the carbon isotopic ratios of our sample as a function of the turn-off mass. The isotopic ratios of the cluster stars analyzed by Gilroy (1989) and Luck (1994) are also shown. In this figure, we decided to plot turn-off mass and not the clump mass, which is a more reliable indicator of the true stellar mass, to facilitate the comparison with previous results. This figure shows that part of our determinations are in good agreement with the relation between $^{12}\text{C}/^{13}\text{C}$ and turn-off mass found by Gilroy (1989). However, it is also clear that some stars have lower $^{12}\text{C}/^{13}\text{C}$ ratios than previously found. In the case of the cluster stars with $M_{\text{TO}} \sim 2.0 M_{\odot}$, we find additional stars with low carbon isotopic ratios. The mean ratio for stars in this region is $^{12}\text{C}/^{13}\text{C} = 13.1 \pm 2.6$. The second group of low $^{12}\text{C}/^{13}\text{C}$ stars, however, have higher masses, which cannot be explained by the observational scatter. Four stars in clusters with $M_{\text{TO}} \geq 2.6$

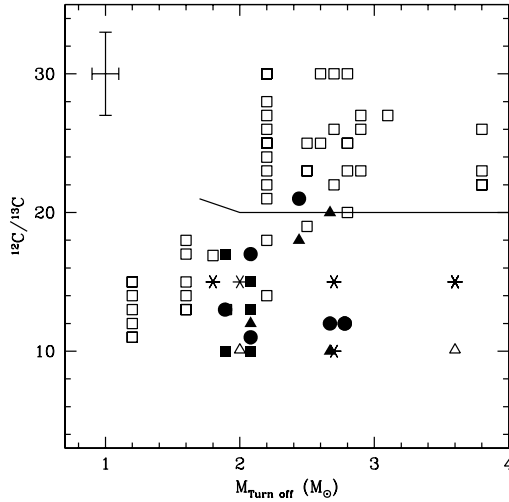


Fig. 16. The carbon isotopic ratio, $^{12}\text{C}/^{13}\text{C}$, as a function of turn-off mass. Stars analyzed in this work are plotted as in the previous figures: the stars analyzed by Gilroy (1989) are shown as open squares, and the stars analyzed by Luck (1994) are shown as starred symbols, or as an open triangle when only a lower limit was available. The theoretical value of $^{12}\text{C}/^{13}\text{C}$ as a function of the initial stellar mass from the models of Schaller et al. (1992) is shown as a solid line.

M_{\odot} have an average of $^{12}\text{C}/^{13}\text{C} = 11.5 \pm 1.0$. These stars, NGC 3532_19, NGC 3532_100, NGC 6281_3, and NGC 6281_4, deviate considerably from other stars in the same mass range. This behavior has not been clearly detected or reported before. This result shows that intermediate-mass stars may also experience an extra-mixing episode, which produces a drop of the $^{12}\text{C}/^{13}\text{C}$ ratio.

In low-mass RGB stars, the low carbon isotopic ratio is attributed to thermohaline mixing operating immediately after the RGB bump (Charbonnel & Zahn 2007a). For intermediate-mass stars, thermohaline mixing is not expected to occur during the RGB because these stars ignite central helium-burning before reaching the bump. However, as suggested by Charbonnel & Balachandran (2000), a similar mechanism might operate in higher mass stars during the early-AGB phase (see also Cantiello & Langer 2008). This effect might explain the observed low $^{12}\text{C}/^{13}\text{C}$ ratio in these stars.

However, when we consider the stellar evolutionary status that we have determined, some difficulties remain. Indeed of the four stars with $M/M_{\odot} \geq 2.0$ and low $^{12}\text{C}/^{13}\text{C}$, only NGC 3532_100 was classified as an early-AGB, the remaining three stars being classified as clump stars. Furthermore, the two stars classified as AGBs with $M/M_{\odot} \geq 2.0$ have high $^{12}\text{C}/^{13}\text{C}$ (NGC 3532_670 and NGC 6633_78). This could imply that not all of these stars will develop a low $^{12}\text{C}/^{13}\text{C}$ ratio. As discussed by Charbonnel & Zahn (2007b), thermohaline mixing could indeed be inhibited by fossil magnetic fields in stars that are descendants of Ap stars. On the other hand, one should also keep in mind that a reliable classification of these stars is not an easy task and this could affect our findings.

The $^{12}\text{C}/^{13}\text{C}$ ratio of the four probable RGB stars was determined and found to be low for three of them, IC 4756_28, 38, and NGC 5822_443. In the CMD two of the stars seem to be post-bump giants, which explains their low ratio. However, IC 4756_38 was classified as a pre-bump giant or alternatively as a

clump star in spite of its low $[\text{N}/\text{C}]$. We note that the cluster IC 4756 is affected by differential reddening, which complicates the classification of its member stars.

7. Conclusions

We have reported the observational results of a homogeneous abundance analysis of elements affected by evolutionary mixing in giants of open clusters. Abundances of C, N, O, Na and the $^{12}\text{C}/^{13}\text{C}$ ratio are derived from high resolution, high S/N spectra using spectrum synthesis. Our sample consists of 31 objects, including red giants, clump giants, and early-AGB stars, in 10 open clusters.

The average $[\text{N}/\text{C}]$ ratio of the sample, $[\text{N}/\text{C}] = +0.61$, is in very good agreement with the values predicted by the Schaller et al. (1992) models after the first dredge-up. However, we identify a group of first ascent red giants with average $[\text{N}/\text{C}] = +0.43 \pm 0.04$, which is lower than for the more evolved stars, with $[\text{N}/\text{C}] = +0.63 \pm 0.03$. This result might indicate a real difference in mixing between red giants and clump or early-AGB giants, in contrast to that expected in the standard stellar models, but in agreement with models including thermohaline convection (Charbonnel & Zahn 2007a; Charbonnel et al. in preparation).

A weak trend with mass, in the sense of smaller $[\text{O}/\text{Fe}]$ for higher mass stars, is also suggested. This must however be interpreted with caution because of the observational error bars.

The sodium abundances derived in our sample are between the values $[\text{Na}/\text{Fe}] = -0.08$ and 0.10 dex. We thus do not measure any high sodium overabundance, i.e., values of up to $+0.60$ dex, as previously reported in the literature. However, the strength of our analysis is the range of stellar masses covered by our stars, in between 1.8 and $3.2 M_{\odot}$, in which stellar evolution models predict an increase of 0.10 dex in the surface sodium enhancement as a function of stellar mass. Our results agree with both the continuous increase in $[\text{Na}/\text{Fe}]$ predicted as a function of stellar mass and the predicted amplitude of this increase of 0.10 between 1.8 and $3.2 M_{\odot}$.

The well-known correlation between $^{12}\text{C}/^{13}\text{C}$ and mass, for stars with $M/M_{\odot} \leq 2.5$, is also seen in our results. However, we also discuss for the first time a group of slightly more massive stars with low $^{12}\text{C}/^{13}\text{C}$. Since these more massive stars do not go through the bump while on the RGB, the extra-mixing events that modify their surface abundances do not occur at the same evolutionary phase as for stars with $M/M_{\odot} \leq 2.5$. However, as discussed by Charbonnel & Balachandran (2000), an extra-mixing event might take place in these stars during the early-AGB and could be related to thermohaline convection (see Charbonnel & Zahn 2007a; Cantiello & Langer 2008).

A detailed comparison of these observational results with the predictions of evolutionary models that include the effects of the thermohaline mixing, will be presented in a forthcoming paper.

Acknowledgements. We are indebted to Dr. Daniel Erspamer, former PhD student at Institut d'Astronomie de l'Université de Lausanne, for having carried out the observations. This research has made use of the WEBDA database, operated at the Institute for Astronomy of the University of Vienna and of the Simbad database operated at CDS, Strasbourg, France. R.S. acknowledges a FAPESP PhD fellowship (04/13667-4). R.G., P.N., and C.C. thank the Swiss National Science Foundation for its support.

References

Allende Prieto, C., García López, R. J., Lambert, D. L., & Gustafsson, B. 1999, *ApJ*, 527, 879

- Allende Prieto, C., Lambert, D. L., & Asplund, M. 2001, *ApJ*, 556, L63
- Alonso, A., Arribas, S., & Martínez-Roger, C. 1999, *A&AS*, 140, 261
- Barbuy, B. 1985, *A&A*, 151, 189
- Barbuy, B., Jorissen, A., Rossi, S. C. F., & Arnould, M. 1992, *A&A*, 262, 216
- Barbuy, B., Perrin, M.-N., Katz, D., et al. 2003, *A&A*, 404, 661
- Barbuy, B., Zoccali, M., Ortolani, S., et al. 2006, *A&A*, 449, 349
- Baumgardt, H., Dettbarn, C., & Wielen, R. 2000, *A&AS*, 146, 251
- Baumüller, D., Butler, K., & Gehren, T. 1998, *A&A*, 338, 637
- Becker, W. 1960, *Zeitschrift für Astrophysik*, 51, 49
- Becker, W., Svolopoulos, S. N., & Fang, C. 1976, *Kataloge photographischer und photoelektrischer Helligkeiten von 25 galaktischen Sternhaufen im RGU- und UCBV-System* (Basel: Astronomisches Institut der Universität Basel, 1976)
- Bozkurt, S. 1974, *Revista Mexicana de Astronomía y Astrofísica*, 1, 89
- Bruntt, H., Frandsen, S., Kjeldsen, H., & Andersen, M. I. 1999, *A&AS*, 140, 135
- Cantiello, M. & Langer, N. 2008, *ArXiv e-prints*, astro-ph/0806.4342
- Carretta, E., Bragaglia, A., Gratton, R. G., & Tosi, M. 2004, *A&A*, 422, 951
- Castelli, F. & Kurucz, R. L. 2003, in *Proceedings of the IAU Symposium* 210, ed. N. Piskunov, W. W. Weiss, & D. F. Gray, A20
- Chanamé, J., Pinsonneault, M., & Terndrup, D. 2005, *ApJ*, 631, 540
- Charbonnel, C. 1994, *A&A*, 282, 811
- Charbonnel, C. 1995, *ApJ*, 453, L41
- Charbonnel, C. & Balachandran, S. C. 2000, *A&A*, 359, 563
- Charbonnel, C., Brown, J. A., & Wallerstein, G. 1998, *A&A*, 332, 204
- Charbonnel, C. & Do Nascimento, J. D. 1998, *A&A*, 336, 915
- Charbonnel, C. & Zahn, J.-P. 2007a, *A&A*, 467, L15
- Charbonnel, C. & Zahn, J.-P. 2007b, *A&A*, 476, L29
- Chen, L., Hou, J. L., & Wang, J. J. 2003, *AJ*, 125, 1397
- Clariá, J. J. & Lapasset, E. 1983, *Journal of Astrophysics and Astronomy*, 4, 117
- Clariá, J. J. & Lapasset, E. 1988, *MNRAS*, 235, 1129
- Clariá, J. J., Lapasset, E., & Minniti, D. 1989, *A&AS*, 78, 363
- Clariá, J. J. & Mermilliod, J.-C. 1992, *A&AS*, 95, 429
- Clariá, J. J., Mermilliod, J.-C., Piatti, A. E., & Minniti, D. 1994, *A&AS*, 107, 39
- Clariá, J. J., Piatti, A. E., Lapasset, E., & Parisi, M. C. 2005, *Baltic Astronomy*, 14, 301
- Coelho, P., Barbuy, B., Meléndez, J., Schiavon, R. P., & Castilho, B. V. 2005, *A&A*, 443, 735
- Cohen, J. G., McWilliam, A., Sheckman, S., et al. 2006, *AJ*, 132, 137
- da Silva, L., de La Reza, R., & Barbuy, B. 1995, *ApJ*, 448, L41
- da Silva, L., Girardi, L., Pasquini, L., et al. 2006, *A&A*, 458, 609
- Dearborn, D. S. P., Lattanzio, J. C., & Eggleton, P. P. 2006, *ApJ*, 639, 405
- Decressin, T., Meynet, G., Charbonnel, C., Prantzos, N., & Ekström, S. 2007, *A&A*, 464, 1029
- Dias, W. S., Lépine, J. R. D., & Alessi, B. S. 2001, *A&A*, 376, 441
- Eggen, O. J. 1968, *ApJ*, 152, 83
- Eggen, O. J. 1969, *ApJ*, 155, 439
- Eggleton, P. P., Dearborn, D. S. P., & Lattanzio, J. C. 2006, *Science*, 314, 1580
- ESA. 1997, *The Hipparcos and Tycho Catalogues*, 1239
- Feinstein, A. & Forte, J. C. 1974, *PASP*, 86, 284
- Fernandez, J. A. & Salgado, C. W. 1980, *A&AS*, 39, 11
- Fuhr, J. R. & Wiese, W. L. 2006, *Journal of Physical and Chemical Reference Data*, 35, 1669
- Geisler, D., Smith, V. V., Wallerstein, G., Gonzalez, G., & Charbonnel, C. 2005, *AJ*, 129, 1428
- Gilroy, K. K. 1989, *ApJ*, 347, 835
- Gilroy, K. K. & Brown, J. A. 1991, *ApJ*, 371, 578
- González, J. F. & Lapasset, E. 2002, *AJ*, 123, 3318
- Gratton, R. G., Carretta, E., Eriksson, K., & Gustafsson, B. 1999, *A&A*, 350, 955
- Gratton, R. G., Sneden, C., Carretta, E., & Bragaglia, A. 2000, *A&A*, 354, 169
- Grevesse, N. & Sauval, A. J. 1998, *Space Science Reviews*, 85, 161
- Hamdani, S., North, P., Mowlavi, N., Raboud, D., & Mermilliod, J.-C. 2000, *A&A*, 360, 509
- Herzog, A. D., Sanders, W. L., & Seggewiss, W. 1975, *A&AS*, 19, 211
- Houdashelt, M. L., Bell, R. A., & Sweigart, A. V. 2000, *AJ*, 119, 1448
- Iben, I. J. 1965, *ApJ*, 142, 1447
- Jacobson, H. R., Friel, E. D., & Pilachowski, C. A. 2007, *AJ*, 134, 1216
- Jorissen, A., Van Eck, S., Mayor, M., & Udry, S. 1998, *A&A*, 332, 877
- Kaufer, A., Stahl, O., Tubbesing, S., et al. 1999, *The Messenger*, 95, 8
- Kippenhahn, R., Ruschenplatt, G., & Thomas, H.-C. 1980, *A&A*, 91, 175
- Kopff, E. 1943, *Astronomische Nachrichten*, 274, 69
- Kozhurina-Platais, V., Girard, T. M., Platais, I., et al. 1995, *AJ*, 109, 672
- Lindoff, U. 1972, *A&AS*, 7, 231
- Luck, R. E. 1994, *ApJS*, 91, 309
- Luck, R. E., Kovtyukh, V. V., & Andrievsky, S. M. 2006, *AJ*, 132, 902
- Maeder, A. & Meynet, G. 1991, *A&AS*, 89, 451
- Mashonkina, L. I., Shimanskiĭ, V. V., & Sakhibullin, N. A. 2000, *Astronomy Reports*, 44, 790
- Meléndez, J. & Barbuy, B. 2009, *A&A*, in press, arXiv:0901.4451
- Meléndez, J., Barbuy, B., Bica, E., et al. 2003, *A&A*, 411, 417
- Mermilliod, J.-C., Andersen, J., Latham, D. W., & Mayor, M. 2007, *A&A*, 473, 829
- Mermilliod, J.-C., Andersen, J., Nordstroem, B., & Mayor, M. 1995, *A&A*, 299
- Mermilliod, J.-C. & Mayor, M. 1989, *A&A*, 219, 125
- Mermilliod, J.-C. & Mayor, M. 1990, *A&A*, 237, 61
- Milone, A., Barbuy, B., Spite, M., & Spite, F. 1992, *A&A*, 261, 551
- Mowlavi, N. 1999, *A&A*, 350, 73
- Pace, G., Pasquini, L., & François, P. 2008, *A&A*, 489, 403
- Palacios, A., Charbonnel, C., Talon, S., & Siess, L. 2006, *A&A*, 453, 261
- Pasquini, L., Randich, S., & Pallavicini, R. 2001, *A&A*, 374, 1017
- Pilachowski, C., Sneden, C., Freeland, E., & Casperson, J. 2003, *AJ*, 125, 794
- Prantzos, N., Charbonnel, C., & Iliadis, C. 2007, *A&A*, 470, 179
- Ralchenko, Y., Jou, F.-C., Kelleher, D. E., et al. 2005, *NIST Atomic Database* (version 3.0) (<http://physics.nist.gov/asd>: National Institute of Standards and Technology)
- Randich, S., Sestito, P., Primas, F., Pallavicini, R., & Pasquini, L. 2006, *A&A*, 450, 557
- Recio-Blanco, A. & de Laverny, P. 2007, *A&A*, 461, L13
- Schaller, G., Schaerer, D., Meynet, G., & Maeder, A. 1992, *A&AS*, 96, 269
- Schmidt, E. G. 1978, *PASP*, 90, 157
- Sestito, P., Bragaglia, A., Randich, S., et al. 2008, *A&A*, 488, 943
- Sestito, P., Randich, S., & Bragaglia, A. 2007, *A&A*, 465, 185
- Shetrone, M. D. 2003, *ApJ*, 585, L45
- Shi, J. R., Gehren, T., & Zhao, G. 2004, *A&A*, 423, 683
- Smiljanic, R., Barbuy, B., De Medeiros, J. R., & Maeder, A. 2006, *A&A*, 449, 655
- Smiljanic, R., Porto de Mello, G. F., & da Silva, L. 2007, *A&A*, 468, 679
- Smith, G. H. 1983, *PASP*, 95, 296
- Smith, V. V., Hinkle, K. H., Cunha, K., et al. 2002, *AJ*, 124, 3241
- Sneden, C., Pilachowski, C. A., & Vandenberg, D. A. 1986, *ApJ*, 311, 826
- Spite, M., Barbuy, B., & Spite, F. 1989, *A&A*, 222, 35
- Spite, M., Cayrel, R., Hill, V., et al. 2006, *A&A*, 455, 291
- Stern, M. E. 1960, *Tellus*, 12, 172
- Sweigart, A. V. & Mengel, J. G. 1979, *ApJ*, 229, 624
- Takeda, Y., Zhao, G., Takada-Hidai, M., et al. 2003, *Chinese Journal of Astronomy and Astrophysics*, 3, 316
- Tautvaišienė, G., Edvardsson, B., Puzeras, E., & Ilyin, I. 2005, *A&A*, 431, 933
- Tautvaišienė, G., Edvardsson, B., Tuominen, I., & Ilyin, I. 2000, *A&A*, 360, 499
- Ulrich, R. K. 1972, *ApJ*, 172, 165
- Valenti, J. A. & Fischer, D. A. 2005, *ApJS*, 159, 141
- Vasilevskis, S., Klemola, A., & Preston, G. 1958, *AJ*, 63, 387
- Weiss, A. & Charbonnel, C. 2004, *Memorie della Società Astronomica Italiana*, 75, 347
- Zahn, J.-P. 1992, *A&A*, 265, 115

Appendix A: Equivalent widths

Table A.1. Equivalent widths of the lines used in the abundance analysis of the stars IC 2714_5, IC 4756_12, 14, 28, 38, 69, and NGC 3532_19. Lines with equivalent widths smaller than 10 mÅ and larger than 150 mÅ were not used.

λ (Å)	Elem.	χ (eV)	log gf	2714_5	4756_12	4756_14	4756_28	4756_38	4756_69	3532_19
6154.22	NaI	2.10	-1.560	85.4	73.3	85.5	96.0	68.6	80.0	89.8
6160.75	NaI	2.10	-1.260	103.0	93.5	114.4	114.9	91.9	100.9	105.8
5528.42	MG1	4.34	-0.470	234.9	225.1	246.6	257.3	228.4	212.6	235.4
5711.09	MG1	4.34	-1.750	137.6	127.7	145.8	145.6	125.9	126.0	137.1
5772.15	SiI	5.06	-1.790	91.2	76.9	79.0	78.0	—	—	82.4
6125.03	SiI	5.59	-1.660	45.8	43.3	44.0	55.5	44.4	45.5	55.3
6131.58	SiI	5.59	-1.840	45.9	28.1	38.4	37.2	35.7	34.0	42.2
6131.86	SiI	5.59	-1.770	37.1	32.0	36.6	40.4	33.3	38.1	43.4
6142.53	SiI	5.59	-1.580	52.5	43.7	44.0	45.1	44.8	48.7	49.7
6145.08	SiI	5.59	-1.500	54.8	45.9	47.8	49.2	45.4	48.4	58.3
6155.14	SiI	5.59	-0.890	96.6	93.6	96.8	96.9	92.5	94.7	105.8
5867.57	CaI	2.92	-1.760	50.0	46.7	62.1	63.5	45.8	45.5	52.9
6122.23	CaI	1.88	-0.180	215.8	197.2	228.2	235.4	199.8	198.1	213.4
6156.03	CaI	2.51	-2.580	30.5	18.9	33.8	38.7	18.6	18.6	43.1
6161.29	CaI	2.51	-1.370	—	103.3	—	—	98.5	100.5	120.5
6166.44	CaI	2.51	-1.270	105.7	97.7	119.3	119.8	95.1	97.5	110.5
6169.04	CaI	2.51	-0.800	129.2	123.9	144.7	146.6	120.3	122.2	134.1
6169.56	CaI	2.51	-0.580	147.6	137.1	157.7	160.1	135.3	138.1	149.1
6493.78	CaI	2.51	-0.280	172.2	155.6	178.1	178.9	154.9	162.1	169.3
6499.65	CaI	2.51	-0.970	128.4	121.0	140.1	141.6	116.0	117.7	134.0
5318.34	SC2	1.35	-1.890	45.6	39.6	53.1	48.7	38.8	42.3	50.0
5334.22	SC2	1.49	-2.200	23.6	20.0	32.8	28.6	17.9	20.8	22.4
5145.47	TiI	1.45	-0.590	87.8	78.5	110.0	113.0	77.9	76.3	93.8
5295.78	TiI	1.06	-1.790	48.9	42.7	78.5	79.4	43.3	—	53.5
5299.98	TiI	1.05	-1.750	42.8	39.9	64.7	—	41.7	42.0	49.2
5338.33	TiI	0.82	-2.100	—	32.2	49.2	—	31.9	34.7	38.3
5351.07	TiI	2.77	-0.210	24.8	30.9	48.5	46.7	28.2	27.3	37.6
5766.33	TiI	3.28	0.220	28.0	25.9	36.9	45.3	29.1	—	32.6
6121.01	TiI	1.87	-1.480	22.3	15.7	33.7	42.7	13.9	15.6	23.3
6126.22	TiI	1.06	-1.480	76.5	62.6	98.2	105.5	61.7	62.8	79.8
6497.68	TiI	1.44	-2.070	22.9	19.9	42.6	48.6	18.5	13.0	26.0
5846.27	V1	3.12	0.700	15.7	16.6	24.2	26.1	12.7	9.9	18.6
6002.65	V1	1.05	-1.720	18.4	16.2	36.7	42.7	—	—	—
6039.69	V1	1.06	-0.740	51.0	44.6	80.9	84.7	40.6	38.7	56.6
6111.65	V1	1.04	-0.720	51.7	43.0	87.1	97.5	41.2	42.4	55.7
6119.53	V1	1.06	-0.560	73.5	64.5	94.4	97.0	57.4	58.6	74.1
6135.37	V1	1.05	-0.910	52.4	41.2	81.0	88.6	38.6	40.9	55.0
6150.15	V1	0.30	-1.680	56.9	47.8	98.6	110.5	45.0	43.9	67.1
6504.19	V1	1.18	-0.830	41.6	36.9	61.5	68.0	36.3	33.7	48.1
5303.22	V2	2.27	-2.040	26.4	23.0	37.6	31.3	19.0	26.5	31.0
6028.28	V2	2.48	-1.990	15.8	15.0	18.9	16.4	13.6	12.4	17.3
5122.12	CR1	1.03	-3.240	58.0	49.5	83.9	95.1	49.9	48.5	65.6
5296.69	CR1	0.98	-1.510	152.5	139.3	177.2	180.4	136.0	141.8	155.1
5300.75	CR1	0.98	-2.230	119.2	104.2	134.3	131.5	98.0	102.2	113.7
5304.18	CR1	3.45	-0.770	33.7	29.6	48.1	50.1	31.0	33.7	37.1
5312.88	CR1	3.43	-0.690	53.6	35.4	54.1	55.8	40.4	37.4	47.5
5318.78	CR1	3.43	-0.800	30.4	31.9	52.8	51.2	32.6	32.3	37.3
5329.12	CR1	2.90	-0.140	99.7	102.2	128.1	130.1	100.9	105.5	109.0
5340.44	CR1	3.42	-0.840	—	33.2	50.6	50.4	31.9	35.7	38.0
5348.32	CR1	1.00	-1.370	151.9	140.8	174.6	180.2	138.8	142.8	154.5
5783.07	CR1	3.31	-0.400	69.6	63.2	76.6	77.5	59.8	60.3	63.6
5783.87	CR1	3.31	-0.560	—	—	—	—	—	—	—
5787.99	CR1	3.31	-0.260	81.4	75.2	91.2	87.3	71.7	—	82.7
5788.39	CR1	3.00	-1.720	21.3	21.9	38.1	40.8	18.4	16.5	25.0
5844.61	CR1	3.00	-1.820	24.9	18.4	30.6	36.5	17.4	12.6	25.0
5863.96	CR1	3.11	-1.970	—	—	22.5	25.9	—	—	—
6135.78	CR1	4.80	0.550	34.9	30.1	38.9	43.9	29.7	30.5	40.6
6501.21	CR1	0.98	-3.730	25.4	23.7	44.3	49.5	22.8	21.1	35.3
6630.02	CR1	1.03	-3.240	40.3	—	—	73.9	—	—	—

Table A.1. continued.

λ (Å)	Elem.	χ (eV)	log gf	2714_5	4756_12	4756_14	4756_28	4756_38	4756_69	3532_19
5305.87	CR2	3.81	-2.240	50.1	47.1	—	45.0	41.3	51.4	56.5
5310.70	CR2	4.05	-2.410	31.7	26.7	27.5	25.4	25.8	28.1	35.8
5313.59	CR2	4.06	-1.840	66.8	60.2	57.6	61.0	53.3	62.8	67.7
5334.88	CR2	4.05	-1.750	58.9	54.0	62.1	58.5	54.4	56.8	62.7
5133.69	FE1	4.18	0.140	179.8	169.5	189.0	198.7	171.6	168.3	178.6
5141.75	FE1	2.42	-2.240	139.7	129.2	159.7	146.1	128.3	125.1	144.0
5143.73	FE1	2.20	-3.690	78.4	71.2	104.9	—	69.0	64.3	86.7
5293.97	FE1	4.14	-1.840	62.4	58.8	75.6	71.1	55.7	59.7	67.6
5294.55	FE1	3.64	-2.810	40.1	34.1	56.7	54.1	34.4	36.2	41.8
5295.32	FE1	4.42	-1.670	56.1	42.5	66.8	61.3	49.1	53.1	59.0
5307.36	FE1	1.61	-2.978	154.4	139.5	170.7	165.4	133.3	139.6	155.2
5315.07	FE1	4.37	-1.550	—	—	74.0	75.9	61.3	64.4	77.8
5320.05	FE1	3.64	-2.490	50.2	42.4	59.5	60.0	43.9	44.8	52.5
5321.11	FE1	4.44	-1.090	—	—	79.7	—	—	—	—
5322.05	FE1	2.28	-2.800	112.0	—	126.8	124.4	—	101.5	115.3
5326.79	FE1	4.42	-2.090	36.9	33.5	—	49.6	34.8	35.0	37.9
5339.94	FE1	3.27	-0.720	172.4	162.1	182.9	183.3	161.9	161.3	170.8
5358.10	FE1	3.29	-3.400	—	—	—	—	—	—	—
5367.47	FE1	4.42	0.443	153.5	—	152.5	152.4	—	—	151.3
5369.97	FE1	4.37	0.536	—	—	168.3	170.8	—	—	—
5568.81	FE1	3.64	-2.950	33.6	28.4	41.5	48.9	28.0	30.6	37.3
5759.27	FE1	4.65	-2.070	18.9	16.5	22.6	—	17.9	16.6	19.7
5760.35	FE1	3.64	-2.490	54.2	45.8	60.4	64.7	44.7	46.2	56.9
5775.09	FE1	0.05	-1.298	—	—	—	—	—	—	—
5778.47	FE1	2.59	-3.430	70.2	61.4	81.3	83.2	55.9	60.3	65.7
5784.69	FE1	3.40	-2.532	—	62.0	77.5	75.3	55.1	60.4	65.5
5838.42	FE1	3.94	-2.290	49.2	42.4	60.0	58.0	41.6	42.2	52.9
5849.70	FE1	3.69	-2.990	24.2	29.3	43.4	44.5	29.7	24.8	27.0
5852.19	FE1	4.55	-1.300	75.6	66.8	89.0	—	63.8	66.8	78.5
5853.18	FE1	1.48	-5.270	39.0	33.8	59.7	62.6	32.8	35.2	46.9
5855.09	FE1	4.61	-1.478	—	40.8	50.4	54.2	40.5	41.8	46.0
5856.08	FE1	4.29	-1.328	—	—	—	—	—	—	—
5858.77	FE1	4.22	-2.260	37.6	32.7	42.6	44.9	30.6	31.1	38.5
5859.61	FE1	4.53	-0.600	—	—	—	—	—	—	—
5862.36	FE1	4.53	-0.250	—	—	—	—	—	—	—
6003.03	FE1	3.88	-1.110	118.2	109.6	123.1	124.4	105.8	107.4	121.6
6007.96	FE1	4.63	-0.750	—	—	—	—	—	—	—
6008.58	FE1	3.87	-1.100	—	—	—	—	—	—	—
6015.25	FE1	2.22	-4.680	28.5	23.4	38.1	48.4	23.4	21.0	32.3
6019.36	FE1	3.57	-3.360	22.7	19.3	30.5	34.6	19.5	16.7	24.6
6024.07	FE1	4.55	-0.110	138.4	126.6	134.1	137.9	123.5	126.6	137.0
6027.06	FE1	4.08	-1.089	107.7	95.1	106.7	107.5	90.4	94.8	104.9
6034.04	FE1	4.31	-2.420	30.9	—	29.6	37.1	19.5	20.9	35.2
6035.34	FE1	4.29	-2.590	17.3	15.5	23.6	27.0	17.7	17.8	20.7
6054.10	FE1	4.37	-2.300	24.3	18.7	29.0	29.0	18.7	18.6	26.2
6120.25	FE1	0.91	-5.970	39.0	31.6	59.1	65.9	28.6	27.9	40.0
6151.62	FE1	2.18	-3.299	101.7	91.4	109.7	116.6	86.0	90.5	105.7
6157.73	FE1	4.08	-1.220	106.4	98.6	121.4	121.4	94.8	97.7	119.3
6165.37	FE1	4.14	-1.474	78.3	69.6	87.1	85.5	67.7	69.3	82.4
6173.34	FE1	2.22	-2.880	131.8	116.9	143.3	143.0	109.0	111.7	132.4
6475.63	FE1	2.56	-2.940	114.3	104.4	133.9	130.3	97.9	100.2	118.1
6481.87	FE1	2.28	-2.984	121.9	108.2	134.4	137.2	105.3	103.4	125.1
6483.94	FE1	1.48	-5.650	—	—	—	—	—	—	—
6495.74	FE1	4.83	-0.920	84.1	61.8	80.5	78.8	60.0	65.5	69.8
6496.47	FE1	4.80	-0.610	90.9	92.7	110.3	104.4	87.8	88.7	97.8
6498.95	FE1	0.96	-4.687	113.3	106.3	140.2	142.3	99.8	102.6	125.8
6627.56	FE1	4.55	-1.680	56.6	46.5	60.4	64.4	47.8	48.7	60.7
6633.42	FE1	4.83	-1.490	—	—	62.7	60.6	—	—	—
6633.76	FE1	4.56	-0.799	89.6	88.3	100.0	98.3	88.4	90.3	98.5
6646.98	FE1	2.61	-3.990	48.5	36.7	63.5	69.0	36.9	37.6	54.9
6648.08	FE1	1.01	-5.918	—	—	—	—	—	—	—

Table A.1. continued.

λ (Å)	Elem.	χ (eV)	log gf	2714_5	4756_12	4756_14	4756_28	4756_38	4756_69	3532_19
5132.67	FE2	2.79	-4.110	60.8	49.5	55.2	50.4	50.9	47.9	61.6
5256.94	FE2	2.89	-4.050	56.9	45.4	49.2	49.1	41.5	46.9	55.2
5264.81	FE2	3.23	-3.200	—	73.0	69.7	69.5	67.0	—	—
5325.56	FE2	3.22	-3.160	83.0	69.9	72.6	64.5	66.3	74.3	81.1
5414.08	FE2	3.22	-3.650	60.2	50.5	47.1	42.5	45.8	49.0	55.1
5425.26	FE2	3.20	-3.220	77.8	66.3	—	59.9	61.7	64.8	73.5
6084.10	FE2	3.20	-3.760	53.3	44.8	45.0	39.4	38.9	43.4	50.8
6113.33	FE2	3.22	-4.110	—	32.9	34.8	—	29.8	—	37.5
6129.70	FE2	3.20	-4.600	—	—	—	—	—	—	—
6149.24	FE2	3.87	-2.700	—	54.9	53.1	50.8	51.1	57.8	66.5
6247.56	FE2	3.89	-2.310	89.1	76.2	—	65.9	72.2	79.0	87.6
6369.46	FE2	2.89	-4.150	52.2	42.5	40.8	40.5	38.7	44.3	50.6
6416.93	FE2	3.89	-2.720	67.5	60.6	57.8	58.3	56.3	63.7	70.4
6456.39	FE2	3.90	-2.060	107.3	89.5	81.4	78.8	85.2	92.3	100.4
5301.04	CO1	1.70	-2.080	67.0	64.0	93.3	97.4	62.0	65.3	74.8
5325.28	CO1	4.21	-0.100	26.3	23.1	31.5	31.0	24.5	24.2	27.3
5342.70	CO1	4.00	0.550	56.4	50.8	64.2	61.2	47.3	51.3	56.9
5352.05	CO1	3.56	-0.020	62.7	52.3	72.9	70.7	50.8	53.1	60.8
5359.20	CO1	4.13	0.010	22.2	19.4	23.3	23.3	17.1	18.4	23.0
5369.59	CO1	1.73	-1.730	—	—	—	—	—	—	—
6117.00	CO1	1.78	-2.570	34.8	26.6	50.1	58.1	24.4	25.6	36.3
6490.34	CO1	2.03	-2.580	31.2	22.0	32.5	41.4	19.3	22.3	30.1
6632.47	CO1	2.27	-2.060	38.7	31.2	55.5	58.6	30.3	29.7	44.1
5137.08	NI1	1.67	-1.630	152.2	144.2	165.2	165.0	141.1	147.5	—
5593.74	NI1	3.90	-0.930	71.3	63.9	72.7	73.9	63.8	61.1	72.2
5760.83	NI1	4.09	-0.850	71.1	56.4	71.2	71.2	51.8	55.7	63.7
5847.01	NI1	1.67	-3.480	73.6	63.9	91.8	—	58.4	63.7	77.7
6007.31	NI1	1.67	-3.400	73.2	64.7	82.3	86.8	61.0	61.0	76.2
6053.68	NI1	4.22	-1.110	48.0	35.4	47.7	48.1	35.6	36.8	51.0
6111.06	NI1	4.07	-0.900	64.3	55.4	64.8	66.7	54.1	56.0	63.2
6128.99	NI1	1.67	-3.400	76.4	63.7	89.3	95.4	59.5	63.2	77.1
6130.13	NI1	4.25	-1.030	42.4	33.3	38.5	45.8	34.0	—	43.9
6635.15	NI1	4.40	-0.830	48.0	45.7	51.6	50.5	41.4	40.9	56.9
6643.64	NI1	1.67	-1.980	164.8	150.1	177.2	180.8	144.0	149.1	165.1
5119.12	Y2	0.99	-1.370	52.6	44.1	60.5	63.9	46.1	44.0	63.5
5289.82	Y2	1.03	-1.870	22.8	21.8	37.0	31.0	17.5	24.7	30.8
5330.58	CE2	0.87	-0.280	28.0	22.7	39.6	35.9	20.7	25.7	31.3
6043.39	CE2	1.21	-0.340	15.4	13.0	18.3	21.0	8.2	6.3	18.2
6645.11	EU2	1.37	0.170	41.1	31.3	36.5	38.6	25.4	33.8	42.2

Table A.2. Equivalent widths of the lines used in the abundance analysis of the stars NGC 3532_100, 122, 596, 670, NGC 3680_13, NGC 5822_1, 201, and 240. Lines with equivalent widths smaller than 10 mÅ and larger than 150 mÅ were not used.

λ (Å)	Element	3532_100	3532_122	3532_596	3532_670	3680_13	5822_1	5822_201	5822_240
6154.22	NaI	108.8	81.1	87.7	133.8	91.5	111.5	78.5	113.2
6160.75	NaI	120.2	99.2	106.5	148.9	109.5	125.9	97.3	126.9
5528.42	MG1	250.4	234.8	235.1	277.5	250.1	254.5	226.3	267.9
5711.09	MG1	146.3	129.0	136.5	162.6	129.3	152.9	131.4	151.5
5772.15	SiI	89.2	82.2	88.0	83.6	74.5	79.5	77.4	77.8
6125.03	SiI	60.0	48.8	54.0	—	51.5	59.8	49.0	61.1
6131.58	SiI	45.7	48.1	45.5	41.9	34.2	35.9	35.1	35.3
6131.86	SiI	43.1	25.1	36.0	46.6	33.9	41.2	37.8	41.3
6142.53	SiI	50.0	43.7	49.5	45.4	43.1	43.5	46.1	43.0
6145.08	SiI	60.2	51.4	54.3	54.0	47.2	47.7	49.2	47.5
6155.14	SiI	106.6	93.0	102.0	105.8	94.5	95.2	95.8	94.2
5867.57	CaI	53.3	50.8	51.9	80.6	58.6	69.4	46.4	71.8
6122.23	CaI	228.0	222.8	207.1	284.6	232.8	248.3	207.2	257.7
6156.03	CaI	33.1	35.5	37.7	66.0	38.5	45.4	23.6	47.1
6161.29	CaI	—	110.2	116.1	169.9	—	147.4	106.4	—
6166.44	CaI	120.3	101.0	107.6	145.5	118.2	127.6	100.0	130.1
6169.04	CaI	145.7	122.7	129.3	174.2	143.2	153.9	126.0	157.1
6169.56	CaI	159.9	146.3	147.9	188.9	159.4	168.3	121.5	170.5
6493.78	CaI	181.2	170.9	166.7	207.4	172.5	190.2	158.5	191.1
6499.65	CaI	148.1	127.0	132.1	177.0	138.6	154.9	124.5	154.6
5318.34	SC2	51.2	43.7	55.5	66.9	43.4	54.1	41.4	53.7
5334.22	SC2	26.4	16.2	25.6	48.5	27.8	36.1	18.8	36.0
5145.47	TiI	107.3	86.5	90.6	154.5	108.2	126.3	85.9	127.9
5295.78	TiI	67.6	46.4	55.0	111.2	76.9	91.7	53.2	95.2
5299.98	TiI	—	31.7	47.2	—	—	—	—	—
5338.33	TiI	—	33.7	38.6	—	—	—	—	—
5351.07	TiI	42.4	34.0	38.3	68.8	44.1	51.5	31.7	56.7
5766.33	TiI	34.2	25.7	23.2	55.4	39.8	46.1	28.0	46.1
6121.01	TiI	31.3	19.2	17.7	70.7	38.4	55.0	20.4	57.0
6126.22	TiI	96.8	64.8	70.8	145.3	99.1	120.9	70.5	123.7
6497.68	TiI	40.1	11.0	20.5	85.8	44.5	65.1	20.4	66.4
5846.27	V1	22.3	12.2	16.0	54.2	25.4	35.0	19.4	34.1
6002.65	V1	33.2	—	18.8	74.6	35.4	52.9	18.8	56.6
6039.69	V1	74.6	45.8	48.6	121.5	82.4	99.0	48.8	104.3
6111.65	V1	74.1	45.6	47.0	145.6	95.9	118.2	49.1	125.4
6119.53	V1	88.3	69.0	72.9	135.6	93.0	115.2	64.2	123.0
6135.37	V1	72.2	50.3	47.6	128.5	84.7	105.3	47.8	109.8
6150.15	V1	86.0	56.6	59.8	162.8	105.7	130.8	54.4	—
6504.19	V1	63.1	42.2	40.2	105.0	64.7	84.5	40.4	88.3
5303.22	V2	32.3	23.1	34.8	50.7	25.5	39.4	23.3	38.8
6028.28	V2	18.9	9.1	13.9	25.2	15.9	20.0	11.6	19.0
5122.12	CR1	80.1	61.1	55.6	—	—	—	59.6	—
5296.69	CR1	174.4	149.0	155.6	231.1	170.3	191.8	144.4	200.7
5300.75	CR1	129.4	108.3	116.6	164.4	127.4	144.1	105.0	151.3
5304.18	CR1	41.4	35.8	39.4	74.3	46.5	48.5	33.0	60.8
5312.88	CR1	52.0	46.1	46.4	73.2	52.4	59.9	43.2	64.0
5318.78	CR1	42.6	24.4	38.6	80.2	49.8	58.6	34.3	64.6
5329.12	CR1	119.8	115.6	—	174.6	128.5	140.2	109.7	—
5340.44	CR1	43.7	20.1	39.0	64.8	51.1	53.6	34.7	56.3
5348.32	CR1	172.3	137.9	153.4	223.8	169.7	191.1	145.8	198.8
5783.07	CR1	72.9	62.4	66.3	97.1	75.0	86.3	62.3	88.2
5783.87	CR1	—	—	—	—	—	—	—	—
5787.99	CR1	86.1	76.2	82.0	104.5	86.5	92.2	75.7	97.9
5788.39	CR1	30.6	25.7	—	61.6	34.3	49.6	23.8	47.3
5844.61	CR1	32.3	18.7	17.7	50.4	29.8	39.5	20.1	39.9
5863.96	CR1	—	—	—	33.2	24.2	30.6	—	29.8
6135.78	CR1	40.7	31.9	32.7	54.0	38.7	47.0	34.2	46.9
6501.21	CR1	46.3	22.4	28.6	86.8	49.2	65.9	26.6	—
6630.02	CR1	—	—	—	116.4	—	91.6	—	—

Table A.2. continued.

λ (Å)	Element	3532_100	3532_122	3532_596	3532_670	3680_13	5822_1	5822_201	5822_240
5305.87	CR2	57.5	44.4	58.8	51.0	40.2	47.4	47.7	45.2
5310.70	CR2	31.6	27.3	38.0	32.5	24.2	22.4	27.9	28.2
5313.59	CR2	64.3	62.6	68.7	78.4	51.2	59.3	59.5	58.1
5334.88	CR2	63.0	54.8	67.7	59.6	53.1	51.6	54.2	48.6
5133.69	FE1	201.0	187.0	188.2	230.0	202.3	206.2	179.3	210.9
5141.75	FE1	161.4	136.9	144.6	194.8	154.2	167.6	134.0	171.3
5143.73	FE1	101.7	75.1	84.5	–	–	–	76.4	–
5293.97	FE1	70.0	56.9	68.1	85.1	71.4	76.7	60.3	78.7
5294.55	FE1	48.9	37.4	44.4	74.2	51.0	58.8	39.6	59.5
5295.32	FE1	64.9	51.4	62.2	75.5	59.0	64.7	55.2	64.4
5307.36	FE1	172.5	144.7	158.5	199.7	160.7	178.7	139.6	180.2
5315.07	FE1	85.3	62.7	–	–	72.3	–	67.0	–
5320.05	FE1	61.6	40.5	47.0	74.2	58.9	62.5	41.4	63.4
5321.11	FE1	–	–	73.9	94.7	–	–	68.4	81.2
5322.05	FE1	126.4	–	119.3	155.7	114.4	132.5	104.1	134.0
5326.79	FE1	43.2	36.3	39.5	–	–	51.3	35.0	–
5339.94	FE1	168.0	185.2	173.6	207.6	181.7	190.0	166.1	199.2
5358.10	FE1	–	–	–	–	–	–	–	–
5367.47	FE1	158.2	153.2	–	163.5	150.2	154.9	–	156.3
5369.97	FE1	177.5	–	–	191.8	–	177.3	–	179.8
5568.81	FE1	44.8	31.0	35.3	57.0	43.8	53.8	31.1	48.6
5759.27	FE1	22.4	16.3	17.1	31.3	22.9	26.1	18.1	25.2
5760.35	FE1	64.0	55.4	64.3	74.1	64.2	68.3	48.0	67.7
5775.09	FE1	–	–	–	–	–	–	–	–
5778.47	FE1	78.1	54.5	63.3	99.6	75.7	88.6	62.4	88.3
5784.69	FE1	–	54.3	68.4	90.2	74.9	83.4	61.6	87.3
5838.42	FE1	59.5	–	53.0	74.8	53.6	62.1	46.3	62.7
5849.70	FE1	32.9	22.2	23.8	47.1	34.9	38.8	24.1	40.4
5852.19	FE1	86.9	68.3	74.2	–	–	–	73.5	–
5853.18	FE1	59.5	35.8	42.1	89.2	60.1	74.1	38.9	75.8
5855.09	FE1	52.5	39.2	44.2	60.0	46.0	54.0	45.4	54.8
5856.08	FE1	–	–	–	–	–	–	66.3	–
5858.77	FE1	47.8	33.5	38.6	60.9	39.5	46.8	32.7	47.7
5859.61	FE1	–	–	–	–	–	–	–	–
5862.36	FE1	–	–	–	–	–	–	–	–
6003.03	FE1	129.7	116.0	120.3	138.8	120.2	128.9	111.8	127.7
6007.96	FE1	–	–	–	–	–	–	–	–
6008.58	FE1	–	–	–	–	–	–	–	–
6015.25	FE1	42.1	21.5	24.6	67.5	37.0	52.9	23.2	54.2
6019.36	FE1	32.8	16.1	19.4	50.4	31.6	38.2	20.4	39.9
6024.07	FE1	144.1	125.8	130.2	150.7	131.3	138.5	127.0	136.7
6027.06	FE1	111.5	96.4	106.7	120.2	98.6	110.4	94.8	109.5
6034.04	FE1	–	26.9	18.7	–	31.3	41.7	20.3	40.9
6035.34	FE1	25.7	14.9	16.6	34.8	24.4	31.0	19.3	31.0
6054.10	FE1	31.1	19.2	24.7	42.9	29.2	34.9	21.8	33.4
6120.25	FE1	56.4	33.8	37.4	96.9	59.1	78.5	35.5	79.9
6151.62	FE1	118.5	93.4	101.7	146.5	111.5	129.0	92.8	128.0
6157.73	FE1	–	110.1	116.2	157.3	114.8	–	100.9	–
6165.37	FE1	91.3	73.6	81.1	104.6	83.9	88.6	71.5	90.2
6173.34	FE1	148.2	122.3	133.0	180.2	138.1	158.0	117.1	156.4
6475.63	FE1	135.0	106.0	106.2	165.1	108.5	–	102.9	–
6481.87	FE1	142.2	115.9	120.4	172.5	125.2	149.0	111.1	150.2
6483.94	FE1	–	–	–	–	–	–	–	–
6495.74	FE1	73.8	74.6	72.0	95.4	74.5	–	67.2	88.5
6496.47	FE1	105.6	80.3	90.0	111.5	95.6	107.1	91.1	105.0
6498.95	FE1	143.5	115.7	120.0	202.5	131.8	164.5	106.4	160.8
6627.56	FE1	68.8	49.6	53.3	76.9	59.3	68.4	54.4	68.6
6633.42	FE1	–	34.3	–	–	52.3	–	–	–
6633.76	FE1	100.5	–	102.0	110.8	95.6	101.3	92.9	102.4
6646.98	FE1	66.6	–	49.5	–	54.7	76.8	41.4	79.9
6648.08	FE1	–	–	–	–	–	–	–	–

Table A.2. continued.

λ (Å)	Element	3532_100	3532_122	3532_596	3532_670	3680_13	5822_1	5822_201	5822_240
5132.67	FE2	64.0	–	63.4	59.6	46.4	53.5	52.9	50.8
5256.94	FE2	59.1	–	55.6	–	49.7	–	49.7	–
5264.81	FE2	82.8	81.4	84.4	69.6	62.7	70.1	–	66.3
5325.56	FE2	81.3	86.2	91.4	76.0	65.0	63.1	69.4	64.6
5414.08	FE2	56.2	52.2	57.1	48.1	39.6	48.1	49.5	43.3
5425.26	FE2	–	68.7	74.8	60.2	51.9	59.4	65.8	57.5
6084.10	FE2	54.7	50.3	55.7	49.0	38.6	45.8	43.3	43.2
6113.33	FE2	–	33.9	42.9	–	24.6	30.8	33.4	30.8
6129.70	FE2	–	–	–	–	–	–	–	–
6149.24	FE2	66.3	64.7	68.2	55.9	46.6	48.8	55.8	48.9
6247.56	FE2	86.5	89.0	87.7	62.9	57.7	63.9	75.4	58.6
6369.46	FE2	48.6	41.1	–	37.8	33.2	40.4	43.0	–
6416.93	FE2	69.7	59.7	68.9	60.3	53.8	–	62.5	57.5
6456.39	FE2	96.2	103.6	101.6	74.2	69.0	78.3	89.7	69.9
5301.04	CO1	89.1	59.7	71.7	–	92.9	104.1	70.0	106.3
5325.28	CO1	28.6	18.4	25.4	40.7	31.8	35.1	25.8	35.8
5342.70	CO1	60.2	52.7	51.6	75.3	58.0	65.7	51.6	68.4
5352.05	CO1	69.4	57.6	54.6	85.0	70.9	76.3	55.2	76.3
5359.20	CO1	25.5	–	–	30.5	25.6	27.1	18.1	27.2
5369.59	CO1	–	95.5	99.4	–	–	131.6	–	–
6117.00	CO1	46.3	31.1	33.5	84.0	53.4	68.6	30.1	68.4
6490.34	CO1	44.0	26.5	35.5	85.7	44.6	38.0	22.9	53.2
6632.47	CO1	52.9	35.5	36.4	86.0	54.6	68.2	35.5	69.8
5137.08	NI1	166.6	152.7	157.0	184.7	169.4	167.4	150.3	173.8
5593.74	NI1	76.9	66.5	73.5	85.0	68.9	74.7	62.5	75.0
5760.83	NI1	72.5	66.2	71.7	96.0	67.0	72.9	60.1	75.5
5847.01	NI1	91.0	67.0	73.2	118.5	85.8	100.5	69.1	105.3
6007.31	NI1	88.1	66.2	69.3	107.9	77.2	94.6	64.9	95.5
6053.68	NI1	54.9	44.1	45.1	62.6	48.4	50.5	41.3	52.0
6111.06	NI1	69.8	53.9	59.4	75.0	60.5	68.0	60.3	67.3
6128.99	NI1	97.7	68.1	72.1	127.6	86.8	106.3	70.8	106.1
6130.13	NI1	47.7	39.3	40.1	59.4	42.6	49.3	35.8	43.7
6635.15	NI1	57.9	42.1	51.8	66.9	46.8	56.3	47.5	55.4
6643.64	NI1	181.0	147.3	156.6	213.7	170.6	193.0	151.6	195.4
5119.12	Y2	67.9	52.7	56.1	80.2	58.8	71.8	55.9	69.3
5289.82	Y2	36.6	21.5	33.5	49.2	22.6	38.3	23.2	37.4
5330.58	CE2	33.9	23.8	31.2	64.0	31.4	45.8	24.7	48.7
6043.39	CE2	27.4	14.0	15.6	37.1	18.9	22.1	13.4	25.5
6645.11	EU2	45.7	28.5	30.8	51.8	31.9	43.8	33.2	41.4

Table A.3. Equivalent widths of the lines used in the abundance analysis of the stars NGC 5822_316, 443, NGC 6134_30, 99, 202, NGC 6181_3, 4, NGC 6633_78, and 100. Lines with equivalent widths smaller than 10 mÅ and larger than 150 mÅ were not used.

λ (Å)	Elem.	5822_316	5822_443	6134_30	6134_99	6134_202	6181_1	6181_4	6633_78	6633_100
6154.22	NaI	73.8	95.7	94.6	101.5	105.4	91.8	86.7	125.5	80.8
6160.75	NaI	98.9	114.6	113.2	117.0	121.4	110.0	106.1	138.3	102.1
5528.42	MG1	232.4	246.4	246.4	256.5	256.7	238.8	243.0	271.5	234.4
5711.09	MG1	136.7	146.3	145.7	145.4	147.5	142.8	144.8	160.4	136.7
5772.15	SiI	–	80.4	86.9	85.2	84.6	85.8	89.8	76.8	83.1
6125.03	SiI	47.6	54.8	53.8	49.2	55.5	58.6	60.4	–	49.6
6131.58	SiI	34.6	37.7	41.8	43.3	37.2	42.4	46.0	40.4	39.4
6131.86	SiI	39.7	43.5	39.8	43.4	40.3	44.8	42.5	42.5	38.1
6142.53	SiI	46.6	46.3	50.8	47.7	46.6	51.0	56.3	43.3	48.0
6145.08	SiI	49.8	49.9	54.3	55.4	48.8	58.9	62.8	49.7	51.4
6155.14	SiI	97.2	97.2	106.3	103.7	97.7	105.2	109.5	99.5	101.1
5867.57	CaI	50.7	64.3	56.9	61.8	65.5	55.2	55.6	73.8	51.7
6122.23	CaI	205.2	234.1	217.8	228.2	245.7	223.0	225.4	280.1	209.5
6156.03	CaI	24.1	34.6	26.5	34.4	41.6	26.7	32.8	53.1	24.3
6161.29	CaI	–	131.7	121.1	120.1	136.3	120.9	123.4	165.3	–
6166.44	CaI	103.0	117.9	110.7	118.3	122.6	112.2	115.8	141.1	105.6
6169.04	CaI	125.2	142.6	138.9	143.2	150.5	136.5	137.9	172.7	131.1
6169.56	CaI	140.4	158.4	153.3	160.8	164.6	154.1	158.0	182.6	147.1
6493.78	CaI	154.7	177.7	171.2	175.9	181.1	176.4	179.7	203.3	164.6
6499.65	CaI	120.2	143.1	133.5	136.9	148.4	138.9	135.9	165.8	127.4
5318.34	SC2	42.2	51.6	47.0	52.5	47.4	52.1	55.6	66.0	49.5
5334.22	SC2	10.5	32.3	30.5	33.5	31.7	27.3	26.2	45.9	26.9
5145.47	TiI	86.8	111.0	91.1	107.5	117.5	93.2	91.8	141.3	92.1
5295.78	TiI	50.8	77.1	59.9	72.6	78.5	56.2	58.0	108.7	57.5
5299.98	TiI	43.3	–	55.0	–	–	–	47.0	–	47.4
5338.33	TiI	35.3	–	–	–	–	–	37.8	–	39.3
5351.07	TiI	35.0	46.8	35.8	40.7	48.5	38.2	38.0	66.4	38.0
5766.33	TiI	27.1	35.9	36.4	34.5	41.6	29.4	29.0	54.7	27.6
6121.01	TiI	19.4	41.2	25.9	37.7	46.9	25.5	26.8	75.3	22.8
6126.22	TiI	67.9	101.0	79.6	92.3	104.6	81.6	81.1	140.7	73.9
6497.68	TiI	22.1	45.5	27.9	42.4	52.5	30.4	21.4	80.0	23.5
5846.27	V1	16.7	28.6	18.4	32.9	27.9	17.4	18.8	45.7	14.2
6002.65	V1	–	38.3	–	33.5	45.3	–	19.8	72.2	–
6039.69	V1	51.5	81.2	63.0	79.1	91.0	58.6	55.1	121.4	55.6
6111.65	V1	47.8	92.9	64.3	80.0	105.1	58.5	56.2	142.8	52.1
6119.53	V1	66.8	96.0	77.4	98.7	97.4	79.6	79.6	133.1	73.1
6135.37	V1	46.3	83.6	59.2	75.0	92.8	55.9	58.1	123.4	51.5
6150.15	V1	52.2	101.2	58.0	91.9	116.8	67.5	63.9	155.8	59.1
6504.19	V1	39.3	66.2	54.0	61.2	73.6	50.0	44.5	99.2	43.7
5303.22	V2	22.4	34.0	25.8	31.6	26.9	31.7	34.2	49.0	32.4
6028.28	V2	14.5	18.5	17.9	22.1	19.5	18.8	16.4	27.0	19.3
5122.12	CR1	55.6	86.9	67.0	80.9	94.8	62.4	65.8	–	59.9
5296.69	CR1	146.2	175.3	155.8	169.7	182.7	162.5	166.3	226.4	155.2
5300.75	CR1	104.8	129.9	117.5	124.0	134.0	118.9	118.2	158.5	112.4
5304.18	CR1	37.5	47.4	42.1	48.0	51.8	36.5	39.8	68.5	42.8
5312.88	CR1	44.3	56.0	53.2	58.0	56.2	44.7	47.6	70.9	46.4
5318.78	CR1	37.5	50.3	–	51.0	53.5	37.4	37.0	77.7	39.9
5329.12	CR1	113.1	129.0	–	131.1	134.6	113.3	117.8	158.4	117.7
5340.44	CR1	38.1	49.5	43.9	49.4	53.6	47.3	32.4	65.8	39.5
5348.32	CR1	142.3	174.7	159.4	–	177.0	162.8	162.4	212.3	152.2
5783.07	CR1	66.7	75.8	72.1	80.2	83.8	69.0	70.9	93.5	64.6
5783.87	CR1	–	–	–	–	–	–	–	–	–
5787.99	CR1	77.5	90.6	85.0	93.1	95.6	78.4	87.6	100.8	81.9
5788.39	CR1	21.5	34.8	31.6	34.6	47.2	23.6	29.8	59.8	29.0
5844.61	CR1	17.6	31.5	25.0	32.8	34.5	23.0	20.7	49.6	21.5
5863.96	CR1	–	18.9	–	23.0	32.5	–	–	34.1	–
6135.78	CR1	31.8	42.5	41.7	41.8	44.2	37.0	35.8	55.7	32.7
6501.21	CR1	23.9	–	–	–	–	34.8	30.0	79.5	28.9
6630.02	CR1	–	–	–	–	–	–	–	109.7	–

Table A.3. continued.

λ (Å)	Elem.	5822_316	5822_443	6134_30	6134_99	6134_202	6181_1	6181_4	6633_78	6633_100
5305.87	CR2	49.9	49.9	48.4	55.5	39.2	58.8	57.3	53.4	56.1
5310.70	CR2	29.5	27.3	32.4	30.0	23.5	34.5	41.5	32.3	32.2
5313.59	CR2	65.3	57.6	67.3	64.1	36.4	67.6	70.9	69.0	66.8
5334.88	CR2	58.1	61.5	58.1	59.0	55.3	67.0	69.8	60.3	65.1
5133.69	FE1	179.1	197.9	185.2	201.7	191.4	189.1	186.1	207.8	183.7
5141.75	FE1	122.5	159.4	128.3	159.2	163.3	150.4	150.3	183.2	144.6
5143.73	FE1	79.7	103.0	84.0	—	—	87.5	86.6	—	85.2
5293.97	FE1	62.1	73.6	68.2	75.2	64.0	68.1	70.6	81.9	65.3
5294.55	FE1	30.1	52.6	47.5	54.2	53.5	43.8	45.9	68.5	43.8
5295.32	FE1	57.1	61.5	59.8	65.1	61.7	59.1	61.6	73.1	62.7
5307.36	FE1	138.5	167.0	154.0	164.8	165.9	163.1	159.1	198.4	154.9
5315.07	FE1	67.6	78.3	74.4	71.1	74.6	76.6	—	—	66.5
5320.05	FE1	48.0	59.9	56.5	62.4	—	54.4	—	71.0	52.9
5321.11	FE1	—	—	—	—	—	—	—	90.1	74.6
5322.05	FE1	106.0	125.6	117.9	124.8	125.5	121.0	122.1	149.7	117.9
5326.79	FE1	40.7	—	42.5	—	—	37.0	37.0	—	42.5
5339.94	FE1	160.8	185.5	163.2	175.1	184.9	181.2	181.6	202.2	171.6
5358.10	FE1	—	—	—	—	—	—	—	—	—
5367.47	FE1	—	154.4	155.2	160.7	155.2	157.5	163.0	157.8	152.6
5369.97	FE1	—	170.5	—	—	171.0	—	—	181.5	—
5568.81	FE1	33.3	44.1	42.5	42.0	51.5	38.4	39.0	54.1	37.4
5759.27	FE1	17.6	24.0	22.3	22.9	25.4	19.1	18.6	27.8	20.4
5760.35	FE1	48.3	62.1	59.6	60.4	66.5	54.8	63.9	71.8	53.4
5775.09	FE1	—	—	—	—	—	—	—	—	—
5778.47	FE1	65.1	79.8	72.1	79.8	82.7	71.3	70.5	99.3	67.4
5784.69	FE1	64.4	77.3	67.9	75.9	78.5	70.2	—	92.4	66.9
5838.42	FE1	42.9	55.0	56.8	57.7	58.1	51.7	53.4	68.9	48.7
5849.70	FE1	24.4	33.6	31.7	41.2	40.2	27.0	29.9	48.0	31.5
5852.19	FE1	71.3	—	78.8	—	—	79.4	80.8	—	73.9
5853.18	FE1	35.1	62.4	47.0	54.4	65.1	45.6	45.2	83.7	42.5
5855.09	FE1	43.6	52.8	48.9	53.2	52.5	46.1	—	58.5	44.3
5856.08	FE1	—	—	—	—	—	—	—	—	—
5858.77	FE1	33.5	43.2	31.1	45.3	45.0	36.6	33.4	52.6	39.0
5859.61	FE1	—	—	—	—	—	—	—	—	—
5862.36	FE1	—	—	—	—	—	—	—	—	—
6003.03	FE1	114.8	124.2	120.0	122.0	—	124.6	125.0	138.6	115.3
6007.96	FE1	—	—	—	—	—	—	—	—	—
6008.58	FE1	—	—	—	—	—	—	—	—	—
6015.25	FE1	26.6	42.4	31.8	38.2	46.8	29.6	26.2	67.1	26.2
6019.36	FE1	23.2	30.9	31.8	34.7	37.7	24.0	20.8	47.0	20.8
6024.07	FE1	129.0	134.9	139.1	136.7	137.0	137.5	144.1	147.9	129.8
6027.06	FE1	101.2	106.5	104.2	105.3	106.9	111.7	114.0	117.1	102.6
6034.04	FE1	29.4	34.1	36.5	33.1	37.2	25.0	25.2	41.0	21.9
6035.34	FE1	20.8	22.8	24.4	25.1	30.1	21.4	18.6	36.8	19.4
6054.10	FE1	25.1	30.0	28.2	31.8	33.8	25.7	25.8	38.5	24.4
6120.25	FE1	32.7	65.1	43.3	50.6	68.8	46.6	42.3	91.0	37.5
6151.62	FE1	96.1	116.4	102.0	108.5	116.5	111.3	113.8	139.8	100.3
6157.73	FE1	104.4	120.2	112.0	117.4	—	—	—	—	110.0
6165.37	FE1	75.4	84.9	82.8	90.1	87.2	85.3	89.2	98.8	77.9
6173.34	FE1	121.0	144.9	128.2	141.2	144.4	140.0	144.2	168.9	128.3
6475.63	FE1	101.1	128.9	114.4	114.7	117.2	122.9	119.9	158.7	116.5
6481.87	FE1	111.7	139.4	118.5	129.5	135.9	133.2	133.7	164.2	117.2
6483.94	FE1	—	—	—	—	—	—	—	—	—
6495.74	FE1	65.7	80.8	69.8	73.1	85.2	80.9	76.8	91.3	67.1
6496.47	FE1	86.0	101.1	97.9	98.9	102.0	97.5	97.5	116.7	100.1
6498.95	FE1	103.6	143.8	112.8	131.1	140.7	131.3	130.2	179.6	116.0
6627.56	FE1	51.3	65.1	59.6	64.7	65.1	—	60.8	72.8	58.2
6633.42	FE1	50.9	—	—	—	—	—	—	—	54.8
6633.76	FE1	95.0	98.2	95.8	97.0	99.3	102.5	—	104.7	100.0
6646.98	FE1	40.8	63.7	55.6	61.4	67.9	58.8	—	—	—
6648.08	FE1	—	—	—	—	—	—	—	—	—

Table A.3. continued.

λ (Å)	Elem.	5822_316	5822_443	6134_30	6134_99	6134_202	6181_1	6181_4	6633_78	6633_100
5132.67	FE2	52.8	53.8	53.9	56.6	55.9	61.1	65.7	51.6	55.9
5256.94	FE2	48.6	–	54.5	50.7	–	59.2	63.8	–	52.6
5264.81	FE2	–	71.1	75.1	70.8	67.9	87.6	–	68.0	78.0
5325.56	FE2	70.1	70.4	70.2	74.4	–	85.2	90.7	71.5	80.4
5414.08	FE2	52.1	48.3	49.6	45.8	43.5	61.3	64.5	44.5	53.0
5425.26	FE2	–	62.9	65.4	63.6	59.5	76.6	–	57.7	66.8
6084.10	FE2	45.3	46.4	46.1	–	–	59.4	61.7	46.7	50.5
6113.33	FE2	33.3	32.6	–	37.6	–	41.5	–	37.7	–
6129.70	FE2	–	–	–	–	–	–	–	–	–
6149.24	FE2	–	51.6	56.9	57.0	47.4	66.6	74.2	50.1	59.8
6247.56	FE2	78.2	69.9	–	68.0	62.5	91.2	95.3	60.7	76.8
6369.46	FE2	44.6	42.4	44.2	43.4	35.4	51.8	55.4	38.4	43.4
6416.93	FE2	61.7	59.6	–	61.9	56.6	72.2	74.8	62.7	62.8
6456.39	FE2	89.7	84.4	91.1	89.9	79.3	103.6	106.7	71.7	90.6
5301.04	CO1	67.9	95.0	82.7	88.6	96.8	80.7	80.9	121.5	75.7
5325.28	CO1	24.9	30.5	33.7	37.8	35.5	27.7	26.5	41.4	30.3
5342.70	CO1	–	63.6	57.9	63.7	63.8	59.3	58.8	73.9	57.7
5352.05	CO1	51.0	71.0	66.2	73.0	74.8	67.6	62.5	85.3	63.2
5359.20	CO1	18.1	24.5	–	24.1	–	21.2	21.1	30.9	20.2
5369.59	CO1	–	–	–	–	–	108.1	–	–	–
6117.00	CO1	28.7	54.9	39.1	48.4	60.9	42.0	41.3	82.2	33.2
6490.34	CO1	21.6	46.0	33.9	34.5	47.5	19.1	21.2	67.3	29.5
6632.47	CO1	36.3	57.4	42.2	54.2	59.9	49.9	44.2	80.7	43.5
5137.08	NI1	152.3	172.6	147.7	161.5	–	161.0	162.3	172.9	147.8
5593.74	NI1	67.3	75.1	75.6	76.5	76.4	76.9	78.5	80.1	70.3
5760.83	NI1	59.6	72.9	68.3	72.0	74.1	68.0	79.3	87.2	62.5
5847.01	NI1	65.8	91.7	81.1	89.3	92.0	82.9	81.7	114.7	73.5
6007.31	NI1	68.3	–	75.6	80.8	87.0	78.1	–	104.5	70.6
6053.68	NI1	39.1	45.5	48.6	50.3	53.2	48.2	49.8	58.9	42.1
6111.06	NI1	55.6	68.2	67.2	68.1	70.8	67.4	66.1	73.7	61.7
6128.99	NI1	67.4	93.1	78.0	89.4	95.0	83.5	88.8	119.0	75.7
6130.13	NI1	38.6	46.6	44.0	47.0	44.5	45.2	48.9	46.8	38.7
6635.15	NI1	49.2	56.3	57.0	58.5	57.9	–	58.2	60.0	55.3
6643.64	NI1	150.5	180.8	162.1	172.3	178.8	177.8	174.4	208.8	162.1
5119.12	Y2	52.9	60.4	51.8	58.1	57.7	63.6	67.4	71.2	56.5
5289.82	Y2	24.2	33.4	25.6	31.2	28.0	32.4	35.1	51.8	32.7
5330.58	CE2	27.8	37.5	25.8	29.9	30.7	31.3	33.1	61.8	33.6
6043.39	CE2	14.2	21.2	17.4	20.4	19.3	20.4	18.6	29.5	14.5
6645.11	EU2	24.0	37.8	29.8	33.9	35.2	47.6	46.0	55.4	38.1

Table A.4. Equivalent widths of the additional Fe II lines used in the abundance analysis of the stars NGC 2360_7, 50, 62, NGC 2447_28, 34, and 41, previously analyzed by Hamdani et al. (2000). Lines with equivalent widths smaller than 10 mÅ and larger than 150 mÅ were not used.

λ (Å)	Elem.	χ (eV)	log gf	2360_7	2360_50	2360_62	2360_86	2447_28	2447_34	2447_41
5132.67	FE2	2.79	-4.110	46.1	51.9	49.5	44.7	51.2	46.6	48.5
5256.94	FE2	2.89	-4.050	—	—	—	—	—	—	—
5264.81	FE2	3.23	-3.200	—	—	59.3	63.2	—	76.9	—
5325.56	FE2	3.22	-3.160	71.7	69.7	67.2	65.0	74.6	74.1	72.0
5414.08	FE2	3.22	-3.650	48.8	49.0	40.6	44.3	58.8	—	45.5
5425.26	FE2	3.20	-3.220	70.4	58.5	55.0	—	70.0	62.6	61.3
6084.10	FE2	3.20	-3.760	49.2	—	34.2	—	52.3	45.5	44.1
6113.33	FE2	3.22	-4.110	30.6	28.5	24.9	26.9	35.6	33.6	33.5
6129.70	FE2	3.20	-4.601	—	—	14.8	—	—	—	—
6149.24	FE2	3.89	-2.700	58.0	50.9	51.4	51.7	57.4	57.5	55.1
6247.56	FE2	3.89	-2.310	73.0	74.6	62.6	69.8	82.1	77.9	75.9
6369.46	FE2	2.89	-4.150	41.1	30.5	28.6	—	42.6	41.5	39.9
6416.93	FE2	3.89	-2.720	57.8	54.7	55.7	—	62.2	57.5	60.6
6456.39	FE2	3.90	-2.060	—	84.4	78.3	82.7	—	91.6	97.1

